



Norwegian University of  
Science and Technology

# Efficient catalysts for achieving NO /NO<sub>2</sub> equilibrium

**Mads Alexander Lid**

Chemical Engineering

Submission date: June 2016

Supervisor: Magnus Rønning, IKP

Co-supervisor: Ata ul Rauf Salman, IKP

Norwegian University of Science and Technology  
Department of Chemical Engineering



# RAMS

Reliability, Availability,  
Maintainability, and Safety

## Efficient catalyst for achieving NO/NO<sub>2</sub>equilibrium

Mads Alexander Lid

June 2016

PROJECT / MASTER THESIS  
Department of Chemical Engineering  
Norwegian University of Science and Technology

Supervisor: Professor Magnus Rønning, IKP

Cospervisor: PhD student Ata ul Rauf Salman

---



# Preface

This masterthesis is a continuation of the specialization course TKP 4510 in Catalysis and Petro chemistry, both written for the department of chemical engineering at the Norwegian University of Science and Technology

The project is affiliated with YARA and Sintef as researc partners During this work, Magnus Rønning was acting supervisor, while Ata ul Rauf Salman from Yara Technology Centre was acting Co-advisor. As this project was in cooperation with Sintef, Senior Scientist Rune Lødeng and Senior Research Scientist Bjørn Christian Enger have also been acting as co-advisors, and David Waller from Yara Technology Centre as industrial partner.

The field of research was selected due to the interest in the interest in process developmentend efficiency, as well as the development of new catalysts.

The goal of this experiment was to synthesize catalyst that could be used oxidation of high concentration nitric oxide, NO, to nitric dioxide, NO<sub>2</sub>. This experiment differs from other previous work for catalytic oxidation of NO due to the use of high concentration of NO.

I would like to thank my supervisor and co-supervisors for their help and ideas in the process. I would also like to give special thanks to Ata ul Rauf Salman and Xavier Auray for their help with academic and laboratory guidance, which is very much apreciated, as well as Cristian Ledesma Rodriguez for helping out with the proper instrumental training. I also want to thank Ole Håvik Bjørkedal for important academic discussions, and all of my other fellow Master students at the Catalysis group for making this a great semester. Finally, I would like to thank Wei Ge for her support and patience during these long office hours.

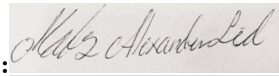
---

Declaration of compliance:

I declare that this is an independent work according to the exam regulations of the Norwegian University of Science and technology (NTNU).

**Place and date:** Trondheim 23.06.16

**Signature:**

A rectangular box containing a handwritten signature in black ink. The signature is cursive and appears to read "M. S. Alexander".

# Sammendrag

Formålet med denne masteren var å karakterisere en Pt/Al<sub>2</sub>O<sub>3</sub> katalysator før og etter post- and pre-modifisering med WO<sub>3</sub>. En 2wt%Ru/Al<sub>2</sub>O<sub>3</sub> og en WO<sub>3</sub>/ZrO<sub>2</sub> katalysator ble også karakterisert. Pt/Al<sub>2</sub>O<sub>3</sub> med 1wt%Pt ble tillaget ved en stegs incipient wetness impregnering. Post- og pre-modifisering av katalysator med 1.3wt %WO<sub>3</sub> skjedde ved to-stegs incipient wetness impregnering. I dette arbeidet har karakterisering med N<sub>2</sub> adsorpsjon, H<sub>2</sub> og CO kjemisorpsjon, røntgenfluorescens (XRF), sveipelektronmikroskopi (SEM), røntgenkrystallografi (XRD), temperatur programmert reduksjon (TPR), Fourier transform infra-red Attenuated Total Reflectance (FTIR-ATR) og in-situ Diffuse Reflectance Infrared Fourier Transform Spectroscopy (DRIFTS) blitt utført.

Nitrogen adsorpsjon viste tilføring av platina og wolframoksid ikke endret overflatearealet, porevolumet eller porestørrelsen til aluminiumoksid. Kjemisorpsjon viste god dispersjon av platina, men denne minket noe etter modifisering med wolframoksid, noe som tyder på blokkering av aktive seter. XRF viser at katalysatoren inneholder 1,2wt%Pt for umodifisert katalysator, mens for både post- og pre-modifisert er innholdet 0.8wt%Pt og 0.7wtWO<sub>3</sub>. Hydrogenopptak ble ikke detektert for TPR, som kan bety at platina allerede er i metallisk form. På grunn av lavt innhold av Pt og WO<sub>3</sub>, samt aluminaoksidets amorfe struktur, kunne hverken face eller krystallstørrelse bestemmes.

Ex-situ FTIR-ATR viste ingen tegn til endring i overflatestrukturen til aluminaoksid etter tilsetning av Pt and WO<sub>3</sub>. DRIFT viser at topper forbundet med sterke og medium sterke Lewis syrer så vidt er synlige for Pt/Al<sub>2</sub>O<sub>3</sub>. Disse toppene har betraktelig sterkere intensitet for både pre- og post- WO<sub>3</sub> modifisert katalysator. Dette kan tyde på at WO<sub>3</sub> øker surheten til aluminaoksid. Disse resultatene vil bli brukt senere for å finne en passende katalysator for det til nå

---

ikke-katalyserte NO oksidasjonssteget i salpetersyre produksjon

# Abstrat

The aim of this work was to characterize an alumina supported Pt catalyst before and after post- and pre-modification with  $\text{WO}_3$ . A 2wt%Ru/ $\text{Al}_2\text{O}_3$  and a  $\text{WO}_3/\text{ZrO}_2$  catalyst were also characterized. Pt/ $\text{Al}_2\text{O}_3$  with a loading of 1wt%Pt was prepared by one step aqueous incipient wetness impregnation. Post and pre-modified 1wt%Pt-1.3wt% $\text{WO}_3$  catalyst was prepared by two step aqueous incipient wetness impregnation. In this work, characterization by  $\text{N}_2$  adsorption,  $\text{H}_2$  and CO chemisorption, X-ray fluorescence (XRF), Scanning electron microscopy (SEM), energy-dispersive X-ray analysis (EDS), X-ray diffraction (XRD), temperature programmed reduction (TPR), Fourier transform infrared Attenuated Total Reflectance (FTIR-ATR) and in-situ Diffuse Reflectance Infrared Fourier Transform Spectroscopy (DRIFTS) with pyridine adsorption were performed.

Nitrogen adsorption showed that the addition of platinum and tungsten oxide did not alter the surface area, pore size or pore volume of the support. Chemisorption showed a good dispersion of platinum on alumina, but this decreased slightly when modified by  $\text{WO}_3$ , indicating blockage of active sites. XRF measurements shows a metal loading of 1.2wt%Pt for unmodified catalyst, and 0.8wt%Pt and 0.7wt% $\text{WO}_3$  for both post- and pre-modified catalyst. No  $\text{CO}$  uptake were detected by TPR, which could mean that platinum was already in its elemental state. Due to the low Pt and  $\text{WO}_3$  content and highly amorphous alumina, assignment of phase type or calculation of crystallite size with XRD was not feasible. Ex-situ investigation with FTIR-ATR did not detect changes in the surface structure after addition of Pt and  $\text{WO}_3$ .

DRIFT investigations shows that band associated with strong and medium Lewis acid sites are barely present in Pt/ $\text{Al}_2\text{O}_3$  catalyst. By contrast, these bands increased in intensity for post- and pre-modified catalyst. This indicates increased acidity of the alumina after  $\text{WO}_3$  addition. These results will later be

---

used in the investigation of a suitable catalyst for the current non-catalytic NO oxidation step in nitric acid production.

# List of abbreviations and symbols

## Abbreviations

A	Ampere
Al <sub>2</sub> O <sub>3</sub>	Aluminium oxide, also known as alumina
Ar	Argon
ATR	Attenuated total reflectance
BET	Brunauer-Emmet-Teller
BJH	Barrett-Joyner-Halenda
BSE	Backscattered Electrons
CO	Carbon monoxide
CO <sub>2</sub>	Carbon dioxide
DRIFTS	Diffuse Reflectance Fourier Transform Spectra
EDX	Energy-dispersive X-Ray Spectroscopy
EDXRF	Energy Dispersive X-Ray Fluorescence
Ge	Germanium
H <sub>2</sub>	Hydrogen
FTIR	Fourier Transform Infrared spectroscopy
KBr	Potassium bromide
LNT	Lean NO <sub>x</sub> Trap

---

ml <sub>n</sub> /min	milliliter normal per minute
N <sub>2</sub>	Nitrogen
NO	Nitrogen oxide
NO <sub>2</sub>	Nitrogen dioxide
N <sub>2</sub> O	Nitrous oxide
NO <sub>x</sub>	Generic term for the mono-nitrogen oxides NO and NO <sub>2</sub>
O <sub>2</sub>	Oxygen
Pd	palladium
Pt	Platinum
Rh	Rhodium
Ru	Ruthenium
SCFC	Standard Cubic Feet per Hourl
SCR	Selective Catalytic Reduction
SE	Secondary Electrons
SEM	Scanning Electron Microscope
TCD	Thermal Conductive Detector
TPR	Temperature Programmed Reduction
V	Volt
VPT	Pore volume of solution
VS	Volume of solution
XRD	X-Ray Diffraction
XRF	X-Ray Fluorescence
WDXRF	Wavelength Dispersive X-Ray Fluorescence
WO <sub>3</sub>	Tungsten oxide



---

## Symbols

$\beta$	peak width
$\Delta_r H_{298}$	reaction enthalpy at 298K
$\eta$	approach-to-equilibrium factor
$\lambda$	Wavelength
$\mu$	Reduced mass
$\nu$	frequency
$\sigma$	surface tension of liquid nitrogenredje
$\Theta$	contact angle789
$\Theta_x$	angle between the incoming x-rays and the normal to the reflecting lattice plane
$C$	BET constant
$D$	Dispersion
$d$	the distance between two lattice planes
$E$	energy
$h$	Planck's constant
$k$	force constant of vibrating bond
$k_p$	the reaction constant
$K$	A constant in Sherres equation
$< L >$	the dimension of the particle in the direction perpendicular to the reflecting plane
$P$	adsorption pressure
$P_0$	equilibrium pressure of the condensed gas
$p_i$	Partial pressure of species $i$
$R$	the gas constant
$R_\infty$	Reflectance of an infinitely thick layer
$r$	the radius of pores
$r_d$	distance between two atoms
$r_{eq}$	distance between two atoms at equilibrium
$T$	Temperature
$V_0$	volume of gas adsorbed in the first monolayer
$V_a$	total volume of adsorbed gas
$V_n$	molar volume of liquid nitrogen
$\text{Å}$	Ångström

---

# Contents

<b>1</b>	<b>Introduction</b>	<b>1</b>
1.1	Oxidation Catalyst . . . . .	1
1.1.1	NO oxidation catalyst . . . . .	3
1.1.2	Support effect . . . . .	4
1.1.3	Deactivation of platinum . . . . .	4
1.1.4	Modification of support acidity . . . . .	4
1.2	Nitric acid Production . . . . .	5
1.2.1	History . . . . .	5
1.2.2	Technology . . . . .	5
1.2.3	Reactions and thermodynamics . . . . .	6
1.2.4	Reaction mechanism . . . . .	8
<b>2</b>	<b>Theory</b>	<b>9</b>
2.1	Catalyst preparation . . . . .	9
2.1.1	Support . . . . .	10
2.2	BET . . . . .	10
2.3	Hydrogen and CO chemisorption . . . . .	11
2.4	X-Ray Fluorescence . . . . .	13
2.5	Scanning electron microscopy . . . . .	15
2.6	XRD . . . . .	17
2.7	TPR . . . . .	19
2.8	IR Spectroscopy . . . . .	19
2.8.1	Molecular vibrations . . . . .	19
2.8.2	Practical uses . . . . .	21
<b>3</b>	<b>Experimental</b>	<b>25</b>
3.1	Catalyst preparation . . . . .	25

---

3.1.1	Reference catalyst: Pt/Al <sub>2</sub> O <sub>3</sub> . . . . .	25
3.1.2	Catalyst Modification . . . . .	26
3.1.3	WO <sub>3</sub> /ZrO <sub>2</sub> and Ru/Al <sub>2</sub> O <sub>3</sub> . . . . .	27
3.2	Characterization . . . . .	28
3.2.1	BET . . . . .	28
3.2.2	Hydrogen Chemisorption and CO chemisorption . . . . .	28
3.2.3	XRD . . . . .	30
3.2.4	XRF . . . . .	30
3.2.5	SEM . . . . .	31
3.2.6	Temperature Programmed Reduction . . . . .	32
3.2.7	XRD . . . . .	32
3.2.8	Fourier transform infrared spectroscopy . . . . .	32
<b>4</b>	<b>Results</b> . . . . .	<b>37</b>
4.1	Nitrogen adsorption . . . . .	37
4.2	Dispersion . . . . .	38
4.3	X-Ray Fluorescence . . . . .	39
4.4	SEM . . . . .	41
4.5	X-ray diffraction . . . . .	45
4.6	Temperature Programmed Reduction . . . . .	47
4.7	FTIR . . . . .	49
4.7.1	FTIR-ATR . . . . .	49
4.7.2	DRIFTS . . . . .	53
<b>5</b>	<b>Conclusion</b> . . . . .	<b>59</b>
<b>6</b>	<b>Further work</b> . . . . .	<b>61</b>
<b>A</b>	<b>Calculations</b> . . . . .	<b>71</b>
A.1	Catalyst preparation . . . . .	71
A.2	Pre-Modification . . . . .	73
A.3	Post-Modification . . . . .	74
<b>B</b>	<b>Pore volume</b> . . . . .	<b>77</b>
<b>C</b>	<b>Nitrogen adsorption</b> . . . . .	<b>79</b>
<b>D</b>	<b>Chemisorption</b> . . . . .	<b>83</b>
D.1	Chemisorption Sequence . . . . .	83

---

D.2	
Chemisorption Isotherm . . . . .	84
<b>E X-ray Diffraction</b>	<b>87</b>
<b>F FTIR wavelength</b>	<b>91</b>
<b>G Risk assesment</b>	<b>93</b>



# List of Figures

1.1	Proposed reaction mechanism of reducing $\text{NO}_x$ storage and reduction in LNT [42]. . . . .	3
2.1	Langmuir isotherm for different surface energies, where $b_1$ is smaller than $b_2$ , $b_2 < b_3$ , etc.[78]. . . . .	12
2.2	An illustration of the method for obtaining only irreversible adsorption, or chemisorption.[78]. . . . .	13
2.3	An illustration of the isotherm of the first test in black, the isotherm for the second test in white and the difference in grey[78]. . . . .	13
2.4	An illustration of transition of an electron and emitting of a photon [1]. . . . .	14
2.5	The interaction between the electron beam and the sample. As can be seen, a number of signals are emitted. . . . .	16
2.6	Example of SEM using SE, BSE, YAG-BSE and EDX . . . . .	17
2.7	An illustration of x-rays scattered by atoms in the ordered lattice structure, as well as the angle of the diffraction [11] . . . . .	18
2.8	The interatomic potential of a diatomic molecule, as HCl, where the curvature is dependent on the bond-vibrations and the energy levels of the molecule. . . . .	22
2.9	Schematics of an ATR setup with the sample placed on top of the ATR crystal. The laser, represented by the red line, passes through the crystal total by total internal reflection, creating an evanescent wave which penetrates the sample, represented by the orange layer. . . . .	23
3.1	Block diagram of preparation method for reference catalyst. . . . .	26

3.2	Block diagram of post-modification method for preparation of modified catalyst. . . . .	27
3.3	Block diagram of pre-modification method for preparation of modified catalyst. . . . .	27
3.4	SEM set-up. . . . .	31
3.5	Flow sheet of the set-up used for the experiment. . . . .	34
4.1	??Platinum catalyst with high amount of small surface particles and 4.1(b) with smaller amount of large surface particles. . . . .	42
4.2	4.2(a)Post-modified catalyst with high amount of small surface particles and 4.2(b) with smaller amount of large surface particles. . . . .	43
4.3	4.3(a)Particle size on pre-modified catalyst with and 4.3(b) a variety of particles of different size. . . . .	43
4.4	Composition of particles on 4.4(a) post-modified catalyst and 4.4(b) pre-modified catalyst. As can be seen, particles consists mainly of platinum with small amounts of tungsten. . . . .	44
4.5	4.5(a) The distribution of platinum and 4.5(b) tungsten in the interior structure of crushed post-modified catalyst.4.5(c) The distribution of platinum and4.5(d) tungsten particles in pre-modified catalyst. . . . .	45
4.6	XRD results for all plots $\theta$ . . . . .	46
4.7	XRD plot for Pt-W $\theta$ . . . . .	47
4.8	TPR of Pt/Al <sub>2</sub> O <sub>3</sub> . . . . .	48
4.9	ATR-spectrum 4000-400 cm <sup>-1</sup> . . . . .	49
4.10	ATR-spectrum 4000-3500 cm <sup>-1</sup> . . . . .	50
4.11	ATR-spectrum 2750-1500cm <sup>-1</sup> . . . . .	51
4.12	ATR-spectrum 1500-400cm <sup>-1</sup> . . . . .	52
4.13	DRIFTIR-spectrum of Al <sub>2</sub> O <sub>3</sub> in the region of 4000-500cm <sup>-1</sup> . . . . .	53
4.14	IR-spectrum 1375:1640 cm <sup>-1</sup> . . . . .	54
4.15	IR-spectrum 1700-1500 cm <sup>-1</sup> for Pt/Al <sub>2</sub> O <sub>3</sub> , Pt-W/Al <sub>2</sub> O <sub>3</sub> and W-Pt/Al <sub>2</sub> O <sub>3</sub> . . . . .	55
4.16	IR-spectrum 1400-1500 cm <sup>-1</sup> for Pt/Al <sub>2</sub> O <sub>3</sub> , Pt-W/Al <sub>2</sub> O <sub>3</sub> and W-Pt/Al <sub>2</sub> O <sub>3</sub> . . . . .	56
4.17	DRIFTIR-spectrum of the OH and CH region for Pt/Al <sub>2</sub> O <sub>3</sub> , Pt-W/Al <sub>2</sub> O <sub>3</sub> and W-Pt/Al <sub>2</sub> O <sub>3</sub> . . . . .	58
C.1	The The adsorption/desorption curve for $\gamma$ -Al <sub>2</sub> O <sub>3</sub> . . . . .	80
C.2	Pore size distribution for $\gamma$ -Al <sub>2</sub> O <sub>3</sub> . . . . .	81



D.1	Pt/Al <sub>2</sub> O <sub>3</sub> The isotherm for the total adsorption with trend line in red and the isotherm in green. The blue line represents strongly adsorbed CO. . . . .	85
E.1	XRD plot for pure alumina $\theta$ . . . . .	87
E.2	XRD plot for Pt $\theta$ . . . . .	88
E.3	XRD plot for Pt-W $\theta$ . . . . .	88
E.4	XRD plot for W-Pt $\theta$ . . . . .	89



# List of Tables

3.1	Time and temperature for the reduction step during pretreatment. For both tungsten modified catalysts, same procedure as for CO chemisorption on Pt/Al <sub>2</sub> O <sub>3</sub> was used. . . . .	28
3.2	H <sub>2</sub> Chemisorption analysis conditions and sequences for Pt/Al <sub>2</sub> O <sub>3</sub> . . . . .	29
3.3	Weight percentage of the different samples in KBr. . . . .	35
4.1	The surface area, pore volume and average pore width of calcined $\gamma$ -Al <sub>2</sub> O <sub>3</sub> , reference catalyst, as well as post- and pre-modified catalyst, calculated from N <sub>2</sub> adsorption. The calculations of pore size and pore volume are based on BJH desorption method. . . . .	38
4.2	The dispersion and crystal size of Pt/Al <sub>2</sub> O <sub>3</sub> , Pt-W/Al <sub>2</sub> O <sub>3</sub> , W-Pt/Al <sub>2</sub> O <sub>3</sub> and Ru/Al <sub>2</sub> O <sub>3</sub> calculated by chemisorption of both CO and hydrogen. Dispersion and crystal size are given for strong adsorption unless stated otherwise. . . . .	39
4.3	Element composition for alumina supported Pt catalyst, non-, post- and premodified, alumina supported Ru catalyst and zirconia supported WO <sub>3</sub> catalyst. Each catalyst were analyzed two times, and the middle values are given. Al <sub>2</sub> O <sub>3</sub> and ZrO <sub>2</sub> have a detection limit of 0.01mm and 1.03mm, respectively. . . . .	40
A.1	A summary of measured amounts of chemicals required for preparing catalyst with 1wt%W and 1wt%Pt . . . . .	71
A.2	A summary of measured amounts of chemicals required for preparing catalyst with 1wt%Pt. . . . .	72
A.3	A summary of measured amounts of chemicals required for preparing catalyst with 1.3wt%WO <sub>3</sub> and 1wt%Pt. . . . .	74

---

A.4	A summary of measured amounts of chemicals required for modification of $WAl_2O_3$ with 1wt%Pt. . . . .	74
A.5	A summary of measured amounts of chemicals required for modification of $PtAl_2O_3$ with 1wt% $WO_3$ . . . . .	75
B.1	Data used for finding pore volume of alumina. . . . .	77
B.2	Data used for finding pore volume of $W/Al_2O_3$ . . . . .	78
D.1	H2 Chemisorption Analysis conditions and sequences for $Pt/Al_2O_3$ . . . . .	83
D.2	CO Chemisorption Analysis conditions and sequences for $Pt/Al_2O_3$ . . . . .	84
D.3	H2 Chemisorption Analysis conditions and sequences for $Ru/Al_2O_3$ . . . . .	84
F.1	Position of pyridine bands upon adsorption on $\gamma$ -alumina . . . . .	92

# Chapter 1

## Introduction

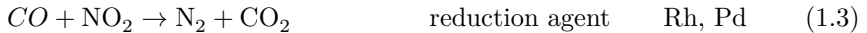
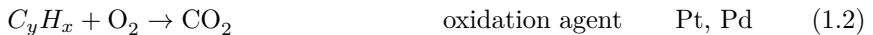
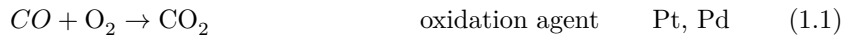
### 1.1 Introduction to Oxidation Catalysis in $\text{NO}_x$ Reduction

Air pollutant acts as one of the major problems regarding air quality in dense populated urban areas. Especially in areas with stagnant air, concentration of pollutants can reach critical levels. The main source of pollutions is a result of combustion processes of fossil fuel in vehicles, power plants and other industrial processes, and these have therefore been given special attention for the past years [67]. Of the air pollutions affecting human health, the most focus has been on  $\text{NO}_x$  [9], where especially long term exposure has proved a negatively effect on health.

As  $\text{NO}_x$  has the ability to react with other chemicals, being responsible for several other air-born components, these are considered primary pollutions. Some of the more critical by-products are photochemical smog, acid rain and tropospheric ozone, where the latter can react further, creating free radicals, which is another health issue. It is also known that  $\text{NO}_x$  contributes to the global warming when forming  $\text{N}_2\text{O}$  [67]. Several attempts have been tried to minimize the amount of  $\text{NO}_x$  release in both industry and in car engines. For industry, usually three methods are used; Pre-combustion, combustion modifications and post-combustion techniques. Pre-combustion is simply the purification of fuel to reduce the content of nitrogen containing species, as this will reduce the

fuel bound  $\text{NO}_x$  formation [22]. On the other hand, combustion modification is the attempt of reducing emissions during incineration processes. This can be achieved by reducing flame temperature, creating oxygen deficient stoichiometry conditions or by changing residence time within different parts of the combustion zone [30, 24].

Post-combustion, as the name implies, concentrates on removal of already formed  $\text{NO}_x$  species after combustion, providing a noticeable reduction of NO [67]. For gasoline vehicle, the three-way catalyst is the main component for  $\text{NO}_x$  removal, where the reduction of NO by CO is the main reaction [64]. Usually, the standard three-way catalyst uses a combination of Pt, Rh and Pd precious metals [20]. Overall main reactions can be seen in equation 1.1, 1.2 and 1.3.



Diesel engines have the highest fuel efficiency at oxygen rich, or lean, conditions, resulting in a lowered fuel consumption, as well as decreasing CO, HC and  $\text{CO}_2$  emissions. Unfortunately, this also removes the reducing agent in the flue gas, meaning that the three-way catalyst cannot be utilized [48]. Instead, other  $\text{NO}_x$  reduction technologies have been commercialized in its place. One such technology is Selective Catalytic Reduction, SCR, using ammonia or urea as the reducing agent. Still, there are challenges connected to this, as transport of reducing agent in a separate tank and consequences of ammonia slip.

The Lean  $\text{NO}_x$  Trap, LNT, on the other hand, do not need an external reducing agent, but rather exploits a two-step cyclic operation; one step with a lean phase, trapping  $\text{NO}_x$ , and reduction during the second, rich phase.  $\text{NO}_2$  is here trapped as surface nitrates by alkaline earth metals in the form of oxides or carbonates. Since the alkaline earth metals' ability to store  $\text{NO}_2$  is more facile, NO must undergo an oxidation step for increased efficiency [7]. Usually, a noble catalyst is used for this step, even though several other catalysts have been proposed [42]. Figure 1.1 represents a proposed mechanism for LNT using Pt as oxidation and reduction catalyst.

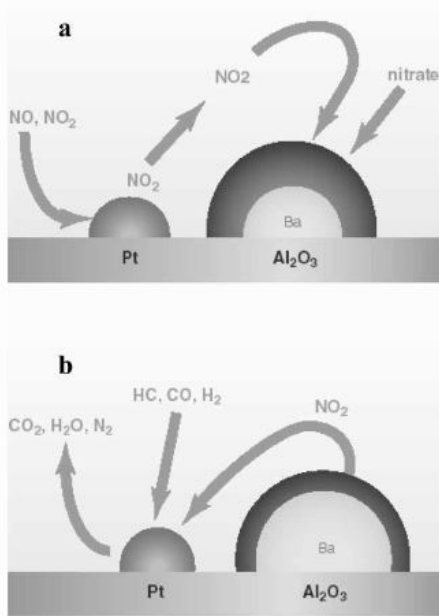


**Figure 1.1:** Proposed reaction mechanism of reducing NO<sub>x</sub> storage and reduction in LNT [42].

### 1.1.1 NO oxidation catalyst

Nitrogen oxides have long been known for their harmful effect on environment and health due to its ability to form smog, ground ozone and acid rain. This has forced governments all over the world to introduce new and strict regulations regarding NO<sub>x</sub> emissions. For this reason, a great deal of oxidation catalysts have been studied for NO oxidation, ranging from supported metal oxides and noble metals to ion exchanged zeolites and activated carbon fiber[46]. Historically, supported noble metals are most commonly used, as they are associated with an outstanding activity over a range of conditions. Of these, alumina supported platinum seems to be the most active metal catalyst in the lower temperature range of 200-300°C, with conversions reported as high as 95% [8]. Unfortunately, noble metals are also known for their high cost due to their scarcity, as well as being prone to a large number of poisons[2, 10, 25, 59].

### 1.1.2 Support effect

The catalytic performance of the supported catalyst is highly dependent on the support material, and has in recent years gained increased attention. Support-metal interactions are not fully understood, but it is believed that the acidic strength of the support material changes the metals catalytic properties. This is especially true for Pt based catalyst, where kinetic studies shows that NO oxidation activity decreases with increased basicity of the support [28, 81, 77]. This is supported by Yazawa et.al. [82], who found that the electron density of unoccupied platinum 5d-orbital decreased with the increased basicity, resulting in more oxidized and less reactive platinum.

### 1.1.3 Deactivation of platinum

As mentioned alumina supported platinum have proven to be the most active metal for NO to NO<sub>2</sub> oxidation. Unfortunately, this seems to be a self-inhibiting process, where both NO<sub>2</sub> and O<sub>2</sub> work as powerful oxidation agents, oxidizing platinum to its non-active form. From the proposed NO oxidation mechanism on platinum, shown in Chapter 1.2.3, oxygen is adsorbed onto vacant sites before it dissociates to chemisorbed oxygen, forming strong oxygen-platinum bonds. Due to the stability of these bonds, an inactive layer of platinumoxide is formed on the surface, inhibiting further reactions [27, 18]. By increasing temperature or oxygen coverage, the oxygen-platinum bond is weakened due to increased steric hinderence, resulting in more reactive oxygen.

It has also been reported that the increase of platinum particle size does have a positive effect on oxidation resistance of platinum [63], as a result of higher stability of platinum oxide on smaller platinum particles [45]. The product, NO<sub>2</sub>, has itself been reported to have an inhibiting effect, as it thermodynamically shifts the equilibrium towards NO formation, but also because of its strong oxidating effect on platinum.

### 1.1.4 Modification of support acidity

As a solution to the self-inhibition of platina, attempts of increasing acidity of alumina in Pt/Al<sub>2</sub>O<sub>3</sub> catalysts have been carried out. X.P. Auray and L. Olsson [2] showed that the addition of chlorine, because of its electronegative nature, decreased the electron density of platinum resulting in higher oxidation



resistance of platinum. They also showed that sulfation increased the acidity of alumina, a trait already used in catalytic cracking. Strong Brønsted acids, which are not seen in pure alumina, were also formed[56]. During catalyst testing, modified catalyst expressed a lower NO oxidation activity than normal, and it was therefore believed that although acidity increased, excess of sulfate and chlorine poisoned the active sites. Luckily, some metal oxide additives have showed promising results for NO oxidation. One such metal oxide is tungsten oxide,  $\text{WO}_3$ [17]. Dawody et.al. discovered that in the absence of  $\text{SO}_2$ ,  $\text{WO}_3/\text{Pt}/\text{AlO}_2$  showed higher NO oxidation prompting than for  $\text{Pt}/\text{Al}_2\text{O}_3$ . According to Zhang et al.[83],  $\text{WO}_3$  addition of tungsten oxide increases the amount of both Brønstedt and Lewis acid sites in alumina support, whereas number of Brønstedt sites increased three times faster than Lewis sites.

## 1.2 The Production of nitric acid

### 1.2.1 History

The production of nitric acid has a long history, where the oldest recipes date back to 1300 in Europe, and maybe earlier in other parts in the world. The use of nitric acid at that time was mostly linked to the art of alchemy, including the creation of aqua regia, a mixture of nitric acid and chloric acid, for dissolving gold. Several production methods developed through the years, where distillation was one of the most important parts in the process. In the middle of the 17<sup>th</sup> century, the Dutch-German alchemist developed a method for production of relatively pure and concentrated nitric acid, where sulfuric acid reacts with saltpeter. This was a technique that would remain unchanged for over a century[32]. In the beginning of the 1800's, the production method changed again with the introduction of sodium nitrate, mainly from Chile. As the source of saltpeter was exhausted by the end of the 19<sup>th</sup> century, new ways for production had to be found [71].

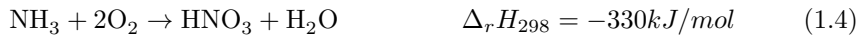
### 1.2.2 Technology

As new and more efficient ways of ammonia productions were introduced, for example the Haber process, the production of nitric acid shifted from using sodium nitrate and sulfuric acid to using ammonia as feedstock. Today, the

production of nitric acid is based on oxidation of ammonia in air which creates nitric oxide. This step does not only yield nitrogen oxide, but does also yield bi-products in the form of Nitrogen gas and nitrous oxide. Nitric oxide is then oxidized by oxygen, before absorption of nitrogen dioxide into water to yield nitric acid. This process is named after Wilhelm Ostwald, who developed and patented it in 1902, although modernized. The overall reaction can be seen in equation 1.4[71].

### 1.2.3 Reactions and thermodynamics

As seen in Equation 1.5, the combustion of ammonia with oxygen is highly exothermic. Still, NO is not the only product formed, which can be seen from equation 1.6 and 1.7. These reactions are undesired, and as they are more thermodynamically stable, they could be avoided by running the combustion at high temperature and low residence time over a platinum/rhodium gauze.



Oxidation of nitric oxide to nitric dioxide is done non-catalytically, and is facilitated by low temperatures, as the reaction is exothermic, see equation 1.8. As nitric dioxide also forms a dimer with itself, low pressure would favor NO<sub>2</sub> before N<sub>2</sub>O<sub>4</sub>. Low pressure also means that this part will occupy a large part of the volume in a process plant[71].



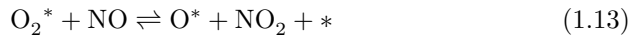
Nitric dioxide is then absorbed into water, creating nitric acid and nitrous acid, where the later will be converted to nitric acid and NO. This process is highly complex, but the overall reaction is shown in equation 1.9. The mass transfer between the gas and liquid phase drives absorption in water. The reason is that

oxidation of nitric oxide is in the gas phase, while absorption of water is in liquid phase[71].



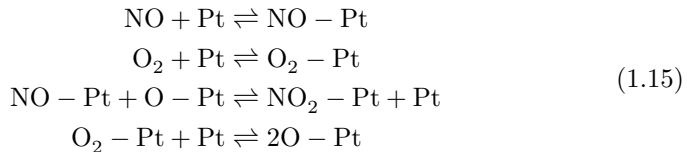
$$(1.10)$$

Even though oxidation of nitric oxide is non-catalytic in the nitric acid production, reaction mechanisms have been proposed for the oxidation of low concentration NO in the presence of a catalyst. This is because NO oxidation is an important step in removal of  $\text{NO}_x$  in exhaust abatement for industry and in diesel engines, especially after combustion in fuel in lean conditions, as it works as an oxidizing agent for noncombusted hydrocarbons. A proposed mechanism for NO oxidation on platinum supported on alumina is as follows:



Here, oxygen is first adsorbed onto a vacant site  $*$ , Equation 1.11, before it dissociates to form chemisorbed oxygen, 1.12. It could also react with chemisorbed NO to form  $\text{NO}_2$ , equation 1.13.  $\text{O}^*$  could also react with non-chemisorbed ceNO to form  $\text{NO}_2$  and a vacant site, Equation 1.14. This step is not a elementary step in itself, but reflects a sequence of quasi-equilibrated elementary steps not shown here[79].

Another reaction model, proposed by Harold et al.[7], see Equation 1.15, also takes into account the strong inhibiting effect of  $\text{NO}_2$ , discussed in Chapter 1.1.3, where  $\text{O}_2$  dissociation is regarded as the ratedetermining step.



### 1.2.4 Reaction mechanism

The oxidation of nitric oxide is rather remarkable, as it is one of the few known third order reactions, which can be seen in equation 1.16.

$$r_{\text{NO}} = -k_p \cdot p_{\text{NO}}^2 \cdot p_{\text{O}_2} \quad (1.16)$$

Where  $p$  is the partial pressure and  $k$  is the reaction constant. Another peculiarity for this reaction is the fact that it is favored by low temperatures both thermodynamically, as well as kinetically, due to the reaction rate constants behavior, which definition can be seen in equation 1.17.

$$\log k_p = \frac{652.1}{T} - 1.0366 \quad (1.17)$$

As mentioned earlier, the oxidation of NO takes place in the gas phase, as well as dimerization of NO<sub>2</sub> [71]. With the use of a catalyst, in this case platinum on alumina, measured oxidation rates for NO oxidation can be expressed with equation 1.18.

$$\log k_p = \frac{k_{pt} \cdot p_{\text{NO}}^2 \cdot p_{\text{O}_2}}{p_{\text{NO}_2}} \cdot (1 - \eta) \quad (1.18)$$

Here  $\eta$  is approach-to-equilibrium factor. The reaction rate is mainly developed for fairly low concentrations of initial NO, and do not necessarily apply of high concentration.

# Chapter 2

## Theory

### 2.1 Catalyst preparation

Heterogeneous catalysts can be mainly divided into two categories; supported catalyst, with small particles on support, and unsupported catalyst, that is, as small loose particles. For supported catalysts, the two most well-known methods for preparing are co-precipitation of the active component and the support, and impregnation of an pre-existing support with a solution containing the active component [12]. Impregnation can again be divided into two categories; dry impregnation, or incipient wetness, and wet impregnation. In dry impregnation, the volume of solution,  $VS$ , corresponds to the pore volume of the support,  $VPT$ , that is  $VPT \geq VS$ [43, 26]. This method relies on penetration of solution by the capillary suction, or forces, due to the small pore diameter in the pores. This method is mostly employed for noble metals, as these are expensive, and a good dispersion of nanoparticles is preferred. A problem occurs when there are weak interactions between a metal precursor and the support surface, as metal complexes can migrate during drying [57]. For wet impregnation, the support is already filled with water, before it is immersed into the solution, taking advantage of the diffusion forces to disperse the active component [43]. Impregnation is followed by drying to evaporate the liquid phase from the sample. Further heat treatment, as calcination, is applied to decompose and remove the nitric oxide precursor and oxidize the support [26].

### 2.1.1 Support

The support used for catalysis should have high surface area, as well as being cheap, inert and have the proper thermal and mechanical stability. Commonly used supports are often oxide supports such as silica, alumina and zeolites. In recent years, also activated carbon has gained more attention. One of the most common oxide supports are aluminum oxide,  $\text{Al}_2\text{O}_3$ , due to being inexpensive and to its high surface area and being inert. The heat treatment of alumina is of high interest and importance, as it will change its transition state depending on the temperature, such as  $\gamma$ ,  $\eta$  and  $\alpha$ - $\text{Al}_2\text{O}_3$ [61]. These transition states have different structure and properties, where  $\gamma$ -alumina is the most used in catalysis, as it has good stability, and at the same time a large surface area [74].

## 2.2 Surface area and pore volume distribution, BET

Nitrogen adsorption is a widely used method for characterization of surface area and pore volume distribution in porous catalysts. The principle behind surface area measurements is quite simple; nitrogen is physisorbed on the surface, and the amount of gas necessary to form one monolayer is measured. By using the cross section of the  $\text{N}_2$  molecule at 77K, which is 16.2 Å, the surface area can easily be found [11].

Usually, the BET isotherm developed by Brunauer, Emmet and Teller gives a good estimate of the surface area, even though it uses an oversimplified model of physisorption[66]. The BET equation 2.1 is a further development of the Langmuir isotherm to describe multilayer formation, and is based on the following assumption.

- Heat of adsorption in the first monolayer is the same for all sites.
- Heats of adsorption for the second and all succeeding layers are equal, and are equal the condensation energy.
- The rate of adsorption and desorption are equal for all layers.

$$\frac{P}{V_a(P_0 - P)} = \frac{1}{CV_0} + \frac{(C - 1) P}{CV_0 P_0} \quad (2.1)$$

where  $P_0$  is the equilibrium pressure of the condensed gas,  $P$  is adsorption pressure,  $V_a$  is the total volume of adsorbed gas and  $V_0$  is the volume of gas adsorbed in the first monolayer. By plotting  $\frac{P}{V_a(P_0-P)}$  as a function of  $\frac{P}{V_a(P_0-P)}$ , a linear relation can be found, where the monolayer coverage can be calculated from the interception of the straight line and the constant  $C$  can be calculated from its slope.

For porous materials, the first part of the isotherm curve follows the same isotherm as for a solid without pores with the same surface area. As adsorption pressure increases, the isotherm seems to deviate away from that of an open surface, indicating filling of pores by capillary condensation. As it occurs below the normal saturation pressure, it indicates formation of liquid-like meniscus in the pores, which can be described by the Kelvin equation 2.2 [66].

$$\ln\left(\frac{P}{P_0}\right) = -\frac{2\sigma V_n \cos\Theta}{rRT} \quad (2.2)$$

Where  $\sigma$  is the surface tension of liquid nitrogen,  $\Theta$  is the contact angle,  $R$  is the gas constant,  $r$  is the radius of the pore,  $T$  is the absolute temperature and  $V_n$  is the molar volume of liquid nitrogen. The most widely used method today is related to the BJH method, where the pores are emptied by step-wise reduction of the adsorption pressure, while taking into account the thinning of the multilayer in pores that are already emptied of condensate [66].

## 2.3 Hydrogen and CO chemisorption

The activity for a supported catalyst often depends on how well the active metal is dispersed on the support, as high dispersion gives high surface area of the active metal. Dispersion is defined as number of available surface sites (active surface metal atoms) divided by the total amount of active sites possible, see 2.3, and is usually given in percentage.

$$D = \frac{\text{number of active sites}}{\text{total amount of active sites possible}} \quad (2.3)$$

A way of measuring the dispersion of a metal is by selective chemisorption. Heterogeneous catalysis involves chemisorption of at least one or more species

involved in the reaction onto the active site, here the metal surface. With higher number of active sites on the catalyst, the greater the probability for one of the species to adsorb to the surface [19].

One way of measuring the dispersion is by selective chemisorption of species that only chemisorbs to the metal surface and not to the support material. Usually, CO and hydrogen are used for this purpose. There are mainly two ways of obtaining chemisorption data; static volumetric chemisorption or dynamic chemisorption. Both methods are based on introducing a known amount of gas, and then plot the quantity adsorbed as a function of the pressure applied. One necessary assumption is that only *one* molecule can chemisorb to one site. The obtained curve is called the chemisorption isotherm. If the chemisorption is not dissociative, most isotherms can be illustrated by the Langmuir isotherm, as seen in Figure 2.1 [78]. The amount chemisorbed does not depend on pressure alone, but also on temperature and surface energy.

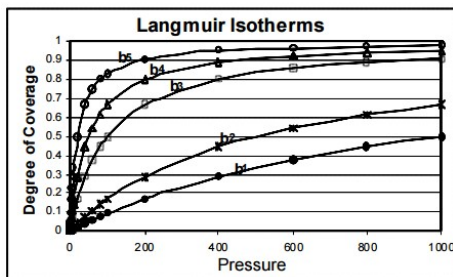


**Figure 2.1:** Langmuir isotherm for different surface energies, where  $b_1$  is smaller than  $b_2$ ,  $b_2 < b_3$ , etc. [78].

In reality, not all of the molecules adsorbed are strongly bound to the metal surface, but will also be adsorbed to the support, or adsorb in multilayers on the chemisorbed species. The weakly bound gas molecules are often reversible adsorption, while the strongly chemisorbed are called irreversible adsorption. After the first adsorption test, the sample is put under vacuum, leaving only the irreversible adsorbed species, before a second adsorption test is done. This is illustrated in Figure 2.2 [78].

The amount of gas adsorbed during the second test will only be reversible adsorbed, and the difference between the isotherm of the first and second test will be the chemically adsorbed species, as seen in Figure 2.3



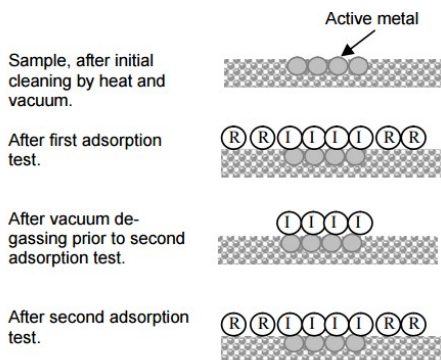


**Figure 2.2:** An illustration of the method for obtaining only irreversible adsorption, or chemisorption.[78].

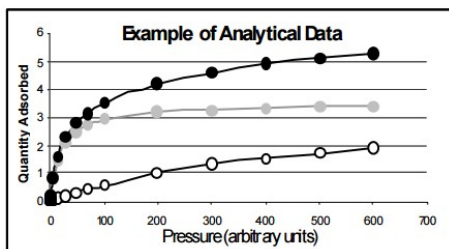


**Figure 2.3:** An illustration of the isotherm of the first test in black, the isotherm for the second test in white and the difference in grey[78].

After finding the linear area of the isotherm, it can be extrapolated to find the monolayer amount of the gas, which will be used further calculations.

## 2.4 X-Ray Fluorescence

X-Ray Rluorescence, or XRF, is an atomic spectrometric method used to determine the element composition of a sample. By using emitted x-rays from a radiated sample as a fingerprint for each element, it is possible to determine the composition. The samples measured are not limited by its form, and can

be powder, solid or liquid. The method is nondestructive to the sample, bulk sensitive and relative fast compared to other characterization methods [1].

XRF is a two-step process method. In the first step, x-rays are emitted from a radiation source, and sent towards the sample. The x-rays emitted need high enough energy to dislodge a tightly bound electron in the inner shell. The atom becomes unstable, and the first step is followed by transition of an electron in an outer shell to an inner shell orbital. The transition is followed by emission of x-ray radiation as the inner shell electron is more strongly bound than in outer shells, thus the name X-ray secondary-emission spectrometer [65]. This can be seen in Figure 2.4. The energy emitted has less energy than the x-ray photon used for dislodging, and corresponds to the difference in the two electron energy levels. The energy intervals between each electron shell are characteristic for an element, so the element can easily be identified. The intensity of the fluorescent photons can be measured at the same time to determine the amount of the element present [1].

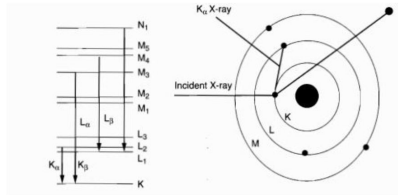


**Figure 2.4:** An illustration of transition of an electron and emitting of a photon [1].

Each shell has its own dedicated symbol, where the inner shell is the k-shell, the second inner is the L-shell and so on. As an electron ejected out of the K-shell is replaced by an electron from another shell, the radiation emitted will be read as K-line. Depending on the origin of the vacancy-filling electron, the line is also dedicated a Greek letter starting with  $\alpha$  for the nearest shell. For example, a K shell vacancy filled by an L-shell electron would give  $K\alpha$ -radiation, as illustrated by Figure 3.5, while a K shell vacancy filled by an M-shell electron would give  $K\beta$ -radiation. For analytical purposes, mainly K- and L-radiation is used for determining elements. One would think that the number of x-ray lines would blur out the spectra, however, the low intensity of the other x-ray lines allows for a clear spectra [1].

XRF can be divided into two groups, wavelength dispersive XRD (WDXRF) and energy dispersive XRD (EDXRF), depending on whether the method is energy or wavelength dispersive. While EDXRF uses detectors that can measure the energy emitted from a sample directly, WDXRF uses an analyzing crystal to disperse the energies in different directions [65].

## 2.5 Scanning electron microscopy

Quite often, the determination of the size and shape of supported particles are of particular interest, e.g. to determine the planes and edges, where the catalyst is most active, or to get a general idea of the structure. Unfortunately, the wavelength of visible light is far greater than of the particles of interest, and an optical microscope will thus be useless for this purpose. Electromagnetic radiation with the proper wavelength does exist, but focusing these waves would be a major issue, due to the need of highly precise optics. Still, we are able to overcome this hindrance by exploiting the wavelike properties of electrons of the pico-meter scale, revealing details down to 0.1 nm [50].

By rastering a narrow electron beam over the surface of the sample, the sample will “emit” secondary and backscattered electrons, which are detected. Knowing the position of the beam, an image of the sample can be made. This is known as Scanning electron microscopy, or SEM. Figure 3.5 gives an overview of what happens when the electron beam hits the sample.

**The secondary electrons** (SE) are mainly low energy electrons at around 5-50eV, and are emitted from close to the specimen surface. Due to this, the SE signal provides information of the surface, as well as topography, giving a 3D image. The contrast is caused by the direction of the scanned surface; if the surface faces the beam, more of the SE are detected, thus appearing brighter than of surfaces pointing away from the detector as seen in Figure 2.6(a). As implied by the name, these are electrons “emitted by the sample”, and not the original electrons from the beam [69].

**The backscattered electrons** (BSE) have a deeper penetration depth, and will therefore contain more information from the bulk of the specimen. This causes the resolution to go down due to elastically scattering. However, it can

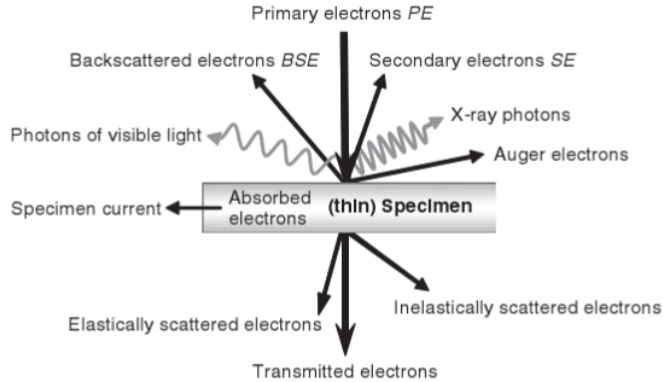


**Figure 2.5:** The interaction between the electron beam and the sample. As can be seen, a number of signals are emitted.

give information about the composition because the BSE signal is related to the atomic weight; the heavier element, the more reflection resulting in a brighter representation in the image. This is demonstrated in Figure 2.6(b) and 2.6(c) [69].

A result of using high voltage electron beam is the ionization of tightly bound inner electrons. The electrons are then ejected from its orbital, followed by relaxation of an electron from a higher shell, causing the emission of an x-ray photon. The X-rays are characteristic for an element, and can be used to determine the chemical composition and dispersion in the sample, as seen in Figure 2.6(d). This is mostly referred to as energy-dispersive X-ray analysis, shortened EDX.[69].

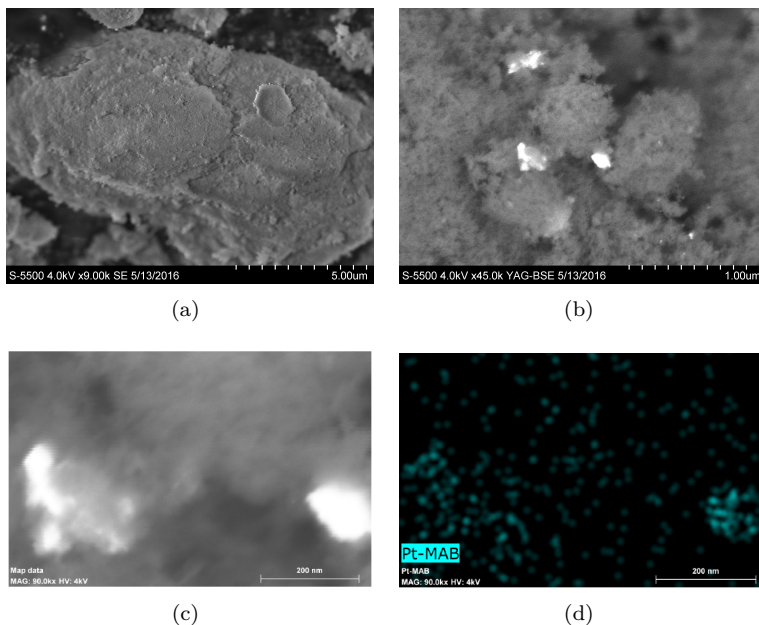


**Figure 2.6:** 2.6(a)The surface of alumina supported platina using SE, 2.6(a) YAG(yttrium aluminium garnet)-BSE, 2.6(c)close-up BSE showing that particles are present and 2.6(d) EDX of the close up surfacesurface, showing that the particles consists of platinum.

## 2.6 X-Ray Diffraction

In catalyst characterization, X-Ray Diffraction ,shortened XRD, is in addition of being one of the oldest, also one of the most used methods. XRD is mainly used for two purposes; the first is the characterization of the crystalline phases by the lattice structures ability to spread the x-ray photons. The patterns of the reflected x-rays are unique for each crystallite structure, and works as a fingerprint. If the monochromatic x-rays are in phase with each other, they will create constructive interference, which, by Bragg's law, Equation 2.4, can be used to calculate the lattice spacing, as well as allowing for further phase identification.

$$n\lambda = 2d\sin\Theta_x; n = 1, 2, \dots \quad (2.4)$$

where  $n$  is the order of the reflection,  $\lambda$  is the wavelength of the x-rays,  $d$  is the distance between two lattice planes and  $\Theta_x$  is the angle between the incoming x-rays and the normal to the reflecting lattice plane. An illustration can be seen in Figure 2.7. Usually, XRD has a detection limit of 1wt% for any given compound [49].

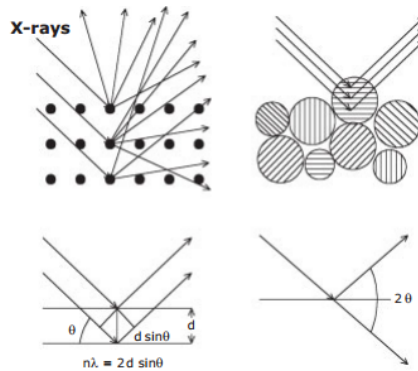


**Figure 2.7:** An illustration of x-rays scattered by atoms in the ordered lattice structure, as well as the angle of the diffraction [11]

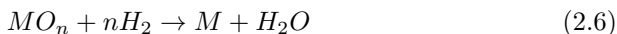
By complementing XRD with line-broadening analysis, the second purpose is expressed; the crystal size can be found. As crystals get larger, the characteristic diffraction peaks will get narrower (or sharper), while smaller crystals tend to get broader and more blurred peaks due to incomplete destructive interference for directions where x-rays are not in phase. To correlate the width of the peak and the crystal size, Scherres formula, equation 2.5, can be utilized [11].

$$\langle L \rangle = \frac{K\lambda}{\beta \cos\Theta} \quad (2.5)$$

Where  $\langle L \rangle$  is a measure of the dimension of the particle in the direction perpendicular to the reflecting plane,  $K$  is a constant often taken as 1 and  $\beta$  is the peak width. The rest of the parameters are as mentioned for Bragg's law.

## 2.7 TPR

TPR, or Temperature-programmed reduction, is an analytical method for monitoring the reduction of a reducible catalyst as a function of temperature. In a typical experiment, the catalyst is exposed to a reducing gas, typically hydrogen, diluted by an inert gas, while the temperature is linearly elevated[16]. The rate of reduction is closely monitored by analyzing the gas mixture at the outlet by either a MS or a Thermal Conductivity Detector (TCD)[51]. The provided information gives the temperature which is needed for total reduction of the catalyst. In addition, TPR also gives information on whether the reduction happens in a single or in multiple steps [11]. A single step reduction is illustrated by Equation 2.6.



The reduction of a catalyst is often a critical step, as lack of proper reduction can eventually lead increased risk of sintering or reduced activity of the catalyst [11]

## 2.8 IR Spectroscopy

IR Spectroscopy is one of the most important and oldest spectroscopic techniques in the field of catalysis. IR spectroscopy is most commonly used in identifying species that are chemisorbed on the catalyst surface, as well as the way these species are adsorbed.

### 2.8.1 Molecular vibrations

The energy of a molecule can roughly be divided into four components: an electronic, a vibrational, a rotational and a translational. A fifth component does also exist, called the nuclear component, but this will not be covered here. A chemical compound has the ability to absorb radiations through energy transitions within these energy components. The vibrational component is based on the chemical bond between atoms in a molecule. As these are not rigid bonds, they have the ability to rotate, vibrate, stretch contract and even bend.

When hit by a photon with a frequency  $\nu$  within the infrared range of 50-2.5  $\mu\text{m}$ , transition between vibrational levels occurs and give rise to absorption bands throughout infrared spectra[52, 14].

Molecular vibrations can be considered as a classical problem in mechanics, where the nuclei,  $N$ , represents the center of mass, and the intramolecular forces holding the molecule together represents massless springs. Within the molecule, each mass needs three coordinates to its position, making  $3N$  degrees of freedom of motion for all the nuclear masses. The molecule itself also needs three coordinates to define its center of gravity, as well as 3 rotational coordinates to define the molecular orientation, meaning there will be six independent degrees of freedom for motion for a non-linear molecule in its equilibrium configuration. This means the molecule will have  $3N-6$  internal degrees of freedom. For a linear molecule, one of the rotational degrees of freedom does not displace the nuclei, and will thus have  $3N-5$  internal degrees of freedom. These internal degrees of freedom correspond to the normal modes of vibrations, and are defined as "when all the atoms in the molecule vibrate with the same frequency and all atoms pass through their equilibrium positions simultaneously"[14], where the center of gravity does not move, even though the vibrations amplitudes of each atom might be of different magnitude and directions

For a diatomic molecule, the deviation from the equilibrium position can be described as a harmonic oscillation, as described in Equation 2.7. The total degrees of freedom will therefore

$$V(r) = \frac{1}{2}k(r_d - r_{eq})^2 \quad (2.7)$$

Where  $k$  is the force constant of the vibrating bond,  $r_d$  is distance between the two atoms and  $r_{eq}$  is the distance at equilibrium. By solving the Schrödinger's wave equation, the corresponding vibrational energy levels, or the energy level for each normal mode is given by Equation 2.8

$$E_n = (n + \frac{1}{2})h\nu \quad (2.8)$$

Where  $n = 0, 1, 2, \dots$  represents the vibrational quantum number,  $h$  is Planck's



constant,,  $\nu$  is the frequency, which can be described by Equation 2.9 and 2.10.

$$\nu = \frac{1}{2\pi} \sqrt{\frac{k}{\mu}} \quad (2.9)$$

$$\frac{1}{\mu} = \frac{1}{m_1} + \frac{1}{m_2} \quad (2.10)$$

Here,  $k$  is the force constant of the bond,  $m_1$  and  $m_2$  are the masses of the vibrating atoms and  $\mu$  is the reduced mass.

In the model of harmonic oscillation approximation, two rules govern the adsorption of a photon; transitions are only allowed if the vibrational quantum number changes by one, that is,  $\Delta n = \pm 1$ , and the transition must lead to a change of dipole moment. This means, that for neighboring vibration levels, the energy is given by 2.11

$$\Delta E_{n+1,n} = \left((n+1) + \frac{1}{2}\right)h\nu - \left(n + \frac{1}{2}\right)h\nu = h\nu \quad (2.11)$$

Whereas the energy of a photon is given by 2.12

$$E_p = h\nu \quad (2.12)$$

Since the only allowed change in vibrational quantum number is by one, a photon would need frequency given by Equation 2.9, giving the molecule an increase in energy equal to  $h\nu$ . As chemical bonds in a molecule are of different strength depending on the atoms, the characteristics of the bond (single bond, double bond etc) and neighboring atoms, each bond will have its own characteristic frequency. The force constant of a bond does not actually correspond to the depth of the interatomic potential, that is, the energy potential of the bond, but its curvature. Still, one can use the frequency to calculate the force constant, as the depth and curvature usually follows each other[52, 14]. This can be seen in Figure 2.8

## 2.8.2 Practical uses

Based on the molecular vibrations, infrared spectroscopy can be used to determine the chemical species present. Several forms of infrared spectroscopy

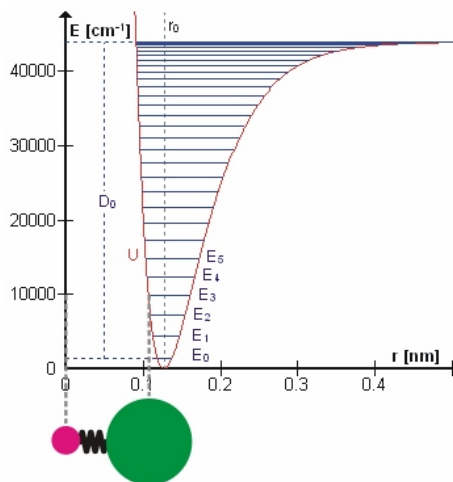


**Figure 2.8:** The interatomic potential of a diatomic molecule, as HCl, where the curvature is dependent on the bond-vibrations and the energy levels of the molecule.

are available today, whereas the most common ones are transmission, Attenuated Total reflection (ATR) and diffuse reflection infrared (DRIFT). Of these methods, the simplest and historically most important is the transmission. In this technique, the sample and an IR transparent matrix is pressed into a self-supporting disc. As electromagnetic radiation within the entire IR spectra is sent through the pellet, some will be absorbed by the sample bulk, before the remaining radiation is sent to a detector. By comparing the received radiation with the transmitted signal, a characteristic spectra of the analyzed compound can be made [52]. ATR on the other hand, is a method for obtaining the spectra of solids and liquids, and a minimum of sample preparation is needed. The sample is placed on top of a prism, or crystal, and a laser beam of monochromatic radiation is sent through the crystal in an angle such that in the sample-crystal interface, it is reflected back into the crystal 2.9.

Along the way, some of the radiation is absorbed by molecular vibrations. By comparing the received signal and the transmitted signal, the characteristic spectra can be found [14]. For DRIFT, the samples can be measured as mere powder, thus eliminating tedious work from sample preparation and diffusion limitations from tightly pressed samples. It is also a good alternative when

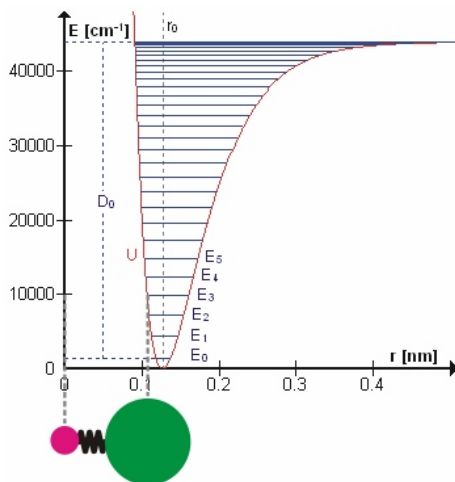


**Figure 2.9:** Schematics of an ATR setup with the sample placed on top of the ATR crystal. The laser, represented by the red line, passes through the crystal total by total internal reflection, creating an evanescent wave which penetrates the sample, represented by the orange layer.

analyzing strongly absorbing or scattering compounds, e.g. oxide supports. When radiation hits the sample, it gets scattered, before it is collected and focused on the detector by ellipsoidal mirrors [52].

As mentioned in Chapter 1.1.4, alumina contains acidic sites that are of great interest, as these could affect the catalytic properties. The acid sites consist of both Brønsted acids and Lewis acids sites, whereas only the Brønsted acid sites can be observed by the hydroxyl vibration of the sites [75]. Lewis acid sites, on the other hand, have coordinatively unsaturated sites, and are thus not a vibrator. A solution of this problem is the use of a probe molecule consisting of a Lewis base. However, not every Lewis base are suitable. The probe has to be small enough to interact with all available sites, and its basic strength should be strong enough to interact to even weak acid sites. However, it should not be so strong that it modifies the structure of the support. One such molecule is pyridine.

The acidic strength of different sites will vary depending on its environment. As a result, also the normal mode will differ for the chemical bonds. As pyridine interacts with Lewis acid sites of different strength, slight changes in the

vibrational levels will occur, leading to absorption of radiation with different wavelengths [55]. The region between  $1700\text{-}1400\text{cm}^{-1}$  is commonly the most studied, as it originate from 8a and 19b ring vibration in the pyridine, which are the most sensitive[36].

# Chapter 3

## Experimental

### 3.1 Catalyst preparation

#### 3.1.1 Reference catalyst: Pt/Al<sub>2</sub>O<sub>3</sub>

A catalyst containing 1wt% Platinum on a  $\gamma$ -alumina support (Pt/Al<sub>2</sub>O<sub>3</sub>) was selected as the reference catalyst. Catalyst was prepared by a one-step incipient wetness impregnation of  $\gamma$ -alumina support with an aqueous solution of Platinum (IV)nitrate, Pt(NO<sub>3</sub>)<sub>4</sub>. Prior to impregnation, Al<sub>2</sub>O<sub>3</sub> was calcined at 750°C for 2.5h.

The incipient wetness point of  $\gamma$ -Al<sub>2</sub>O<sub>3</sub> was estimated by dropwise addition of distilled water. The wetness point was used to calculate the amount of platinum nitrate precursor needed to give 1 wt% Pt, and the precursor solution was prepared thereafter. The solution was homogenized by stirring, before dropwise addition to the support while manually stirring to ensure exposure of all of the  $\gamma$ -Al<sub>2</sub>O<sub>3</sub> support. The wet powder was then dried at 110°C overnight, then lightly crushed to break up clusters of alumina particles and transferred to a fixed bed quartz calcination reactor. The powder sample was heated to 600°C at a ramp of 5°C/min, and calcined under 55mL<sub>n</sub>/min air for 2h at this temperature. This synthesis was based on the work of Xavier P. Auvray and Louise Olsson[2]. A representation of the procedures can be seen in Figure 3.1.

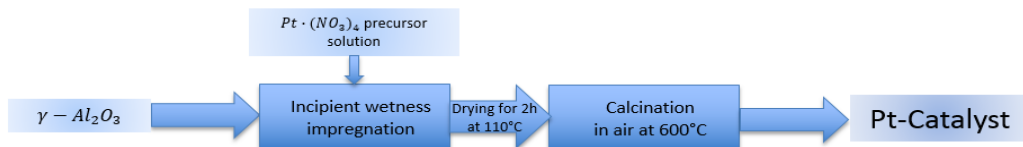


**Figure 3.1:** Block diagram of preparation method for reference catalyst.

### 3.1.2 Catalyst Modification

The reference catalyst was modified with the aim of changing its acidic/basic properties of alumina support. For modification,  $(\text{NH}_4)_{10}\text{W}_{12}\text{O}_{41} \times \text{XH}_2\text{O}$ , or Ammonium tungsten oxide hydrate, was used, based on work on its property to increase the amount of Lewis as well as Brønsted acid sites on the alumina surface [54, 83].

Modified catalyst will hereafter be denoted as X-Y/ $\text{Al}_2\text{O}_3$ , where X denotes the compound from the first impregnation and Y from the second. A representation of the procedures for post- and pre-modification can be seen in Figure 3.2 and 3.3 respectively.

#### Post-modification

The incipient wetness point of Pt/ $\gamma$ - $\text{Al}_2\text{O}_3$  was estimated by dropwise addition of deionized water. The wetness point was used to calculate the amount of Ammonium tungsten oxide hydrate precursor needed to give 1 wt%  $\text{WO}_3$ , and the precursor solution was prepared thereafter. Tungsten salt was dried for 2h at  $100^\circ\text{C}$  to remove any adsorbed water to ensure an accurate estimation of incipient wetness impregnation calculations.

#### Pre-modification

To see whether the modification with tungsten would cover platinum particles or block pores, pre-modification was conducted. Here, the support was first modified with  $(\text{NH}_4)_{10}\text{W}_{12}\text{O}_{41} \times \text{XH}_2\text{O}$ , before addition of platinum, following the procedure mentioned in section 3.1.2 and 3.1.1 respectively.

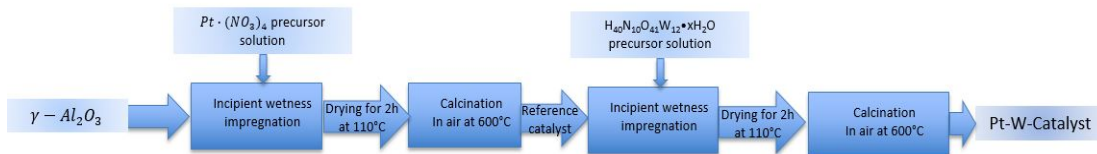


**Figure 3.2:** Block diagram of post-modification method for preparation of modified catalyst.

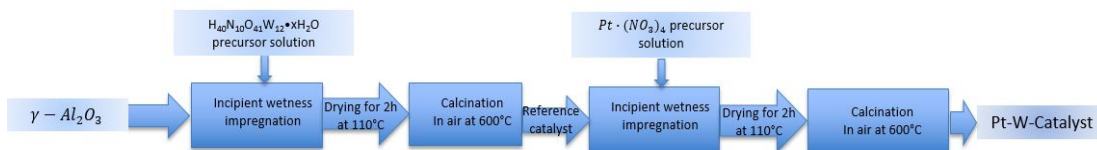


**Figure 3.3:** Block diagram of pre-modification method for preparation of modified catalyst.

### 3.1.3 WO<sub>3</sub>/ZrO<sub>2</sub> and Ru/Al<sub>2</sub>O<sub>3</sub>

Both WO<sub>3</sub>/ZrO<sub>2</sub> and Ru/Al<sub>2</sub>O<sub>3</sub> were commercial catalyst supplied by Alpha Aesar.

## 3.2 Characterization

### 3.2.1 BET

BET surface area was measured by adsorption of nitrogen at  $77K$ , using a Micrometrics TriStar II instrument. The samples were first weighted to be around  $60-80mg$ , and then degassed at  $200^{\circ}C$  overnight. The physiosorption isotherms were obtained, and the BET surface area and pore-size distribution were then found in accordance with section 2.2

### 3.2.2 Hydrogen Chemisorption and CO chemisorption

Dispersion of active metal was measured using a Micrometrics ASAP 2020 instrument. Quartz-wool was first loaded into a U-shaped quartz reactor. Approximately  $150mg$  of catalyst was then introduced, before a second layer of quartz wool was inserted. The reactor was then mounted to the instrument, and placed inside an electrical heated furnace. A thermocouple was placed along the outside of the reactor, at the height of the catalyst, to monitor the temperature. The samples were then evacuated for approximately 2h, before a manual leak-test was conducted. This was done to ensure that the pressure change did not surpass more than  $50\mu mHg/min$ . The automatic sequence was then started. For platinum dispersion measurement, it was assumed that the chemisorption gas did not interact with the support. It was also assumed that no impurities were present, and adsorption only happened at the surface of platinum particles. Time and temperature for the reduction step during pretreatment for the different catalysts is summarized in Table 3.1

**Table 3.1:** Time and temperature for the reduction step during pretreatment. For both tungsten modified catalysts, same procedure as for CO chemisorption on Pt/ $Al_2O_3$  was used.

Sample	Chemisorption gas	Temp[ $^{\circ}C$ ]	Time[min]
Pt/ $Al_2O_3$	Hydrogen	600	120
Pt/ $Al_2O_3$	CO	600	120
Ru/ $Al_2O_3$	Hydrogen	400	120



**Pt/Al<sub>2</sub>O<sub>3</sub>**

For hydrogen chemisorption, the sample was first evacuated with helium for 30min at 110°C and leak tested. A flow of hydrogen was then introduced for 10min at 100°C for in-situ reduction. The sample was then heated at 10°C/min to 600°C under a flow of hydrogen gas for 2h. After reduction, the sample was evacuated for 2h at 600°C and for 30min at 35°C. A leak test was then preformed, before evacuation at 35°C for 20min. This was followed by the analyzing step at 35°C [4].

For CO chemisorption, the sample was first evacuated with helium for 1h at 400°C and leak tested. The sample was then heated at 10°C/min to 600°C under a flow of hydrogen gas for 2h. After reduction, the sample was evacuation for 1h at 580°C and for 45min at 100°C. A leak test was then preformed, before evacuation with helium at 50°C for 1h. This was followed by the analyzing step at 35°C [4].

For illustration, the the analysis sequences for hydrogen chemisorption on Pt/Al<sub>2</sub>O<sub>3</sub> is given in Table 3.2

The same procedures were also used for chemisorption on both Pt-W/Al<sub>2</sub>O<sub>3</sub> and W-Pt/Al<sub>2</sub>O<sub>3</sub>, and the analysis sequences is summarized in TableD.1 and D.2 in Appendix D.1.

**Table 3.2:** H2 Chemisorption analysis conditions and sequences for Pt/Al<sub>2</sub>O<sub>3</sub>.

Task number	Analysis step	Temp[°C]	Time[min]
1	Evacuation	110	30
2	Leak Test	100	
3	Hydrogen Flow	100	10
4	Hydrogen Flow	600	120
5	Evacuation	600	120
6	Evacuation	35	30
7	Leak test	35	
8	Evacuation	35	20
9	Analysis	35	

### **Ru/Al<sub>2</sub>O<sub>3</sub>**

For hydrogen chemisorption, the sample was first evacuated with helium for 2h at 35°C. The sample was then heated at 10°C/min to 400°C and leak tested. A flow of hydrogen gas was introduced for 2h at 400°C for in-situ reduction. After reduction, the sample was evacuation for 2h at 400°C and for 30min at 100°C. A leak test was then preformed, before evacuation at 100°C for 30min. This was followed by the analyzing step. The analysis sequences is summarized in Table D.3 in Appendix D.1

As Ru/Al<sub>2</sub>O<sub>3</sub> came in an egg shell pellet, with a darker outer layer containing ruthenium and a white and, presumably, pure alumina phase in the interior, both pellet and crushed catalyst underwent chemisorption.

### **WO<sub>3</sub>/ZrO<sub>2</sub>**

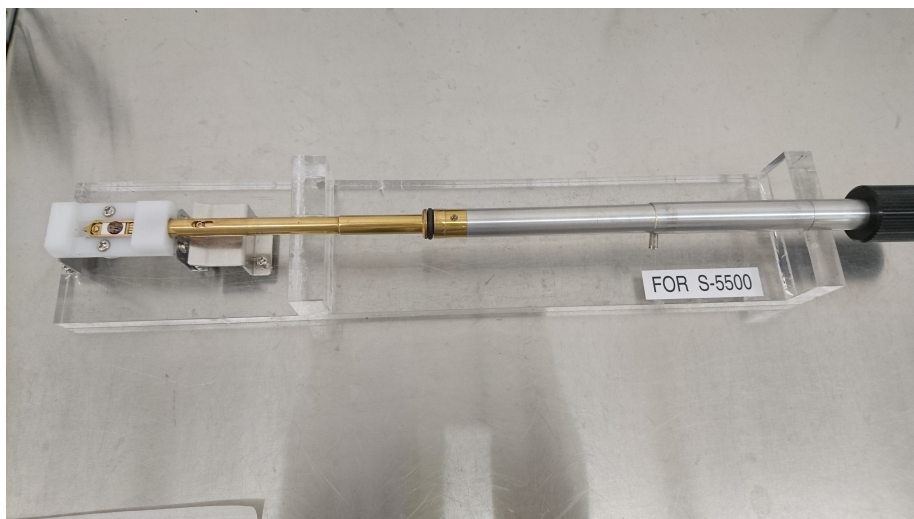
For WO<sub>3</sub> on ZrO and SiO<sub>2</sub>, it has been reported that no chemisorption of H<sub>2</sub> or CO, respectively, takes place [58]. It is therefore assumed that this is also the case for WO<sub>3</sub>/Al<sub>2</sub>O<sub>3</sub>, as reports of this has yet to be found.

### **3.2.3 XRD**

The XRD aparatus Bruker D8 Advanced DaVinci X-Ray Diffractometer – D8 DaVinci1 CuK  $\alpha$  radiation was used for obtaining the XRD profiles spectra. The catalyst was prepared in the second smallest sample holder, with a  $2\theta$  angle of 5° – 75° with 15 seconds steps in 30 minutes with slit opening set to V6.

### **3.2.4 XRF**

For obtaining the composition of the sample, Rigacu Supermini200 instrument was applied. A pellet was first prepared by mixing the approximately 200mg sample with 2.5-3.0g boric acid. The mixture was then pressed into a pellet, which was placed into the pellet-holder, covered with polypropylene film on one side. The weight of the sample and the boric acid was entered into the software, together with the diameter of the pellet.



(a)

**Figure 3.4:** SEM set-up.

### 3.2.5 SEM

Scanning electron microscopy was used to investigate changes in the surface topography of alumina supported Pt-, Pt-W- and W-Pt- catalyst. The imaging was performed in a Hitachi S-5500 Scanning Electron Microscope, using PC-SEM software for image processing. Crushed and uncrushed samples were applied to a metal stub covered with either double layer copper or carbon tape, before being mounted to the sample holder. The sample holder was then entered into the SEM apparatus. The setup is demonstrated in figure 3.4.

Focusing of images was conducted stepwise, with correction of stigmatism and focus alignment between each step for optimization of image quality and resolution. A current of 5A was used to prevent charging effects and voltages between 5V and 3V were chosen, depending on the wanted resolution.

EDX was carried out for element analysis as part of the topographical investigation, and Hitachi S-5500 Scanning Electron Microscope, in collaboration with

Espirit 1.9.4.5 software, was used for this purposes. As EDX measurements utilizes x-ray excitation from the sample, a high current, preferably 20A, is needed to ensure good detection. For topographical reasons, a voltage of no more than 5kV was used.

### 3.2.6 Temperature Programmed Reduction

Temperature Programmed Reduction was carried using ChemBET 300 TPR analysis apparatus. Quartz-wool was first loaded into a U-shaped quartz reactor. Approximately 150mg of catalyst was then introduced, before a second layer of quartz wool was inserted. The tube was then installed in the apparatus, and leak-test performed using the reduction agent, made up of 7% $H_2$  in Argon with a flow of 60mL/min and a pressure of two bars. After leak test, the furnace was installed, and the heating to 800°C at 10°C/min was initiated, still under a flow of 60mL/min 7% $H_2$ /Ar. A thermocouple was inserted to the quartz reactor prior to heating for temperature control. A thermal conductivity detector was used to measure the hydrogen consumption as a function of temperature.

### 3.2.7 XRD

The XRD apparatus Bruker D8 Advanced DaVinci X-Ray Diffractometer – D8 DaVinci1 CuK  $\alpha$  radiation was used for obtaining the XRD profiles spectra. The catalyst was prepared in the second smallest sample holder, with a  $2\theta$  angle of 5° – 75° with 15 seconds steps in 30 minutes with slit opening set to V6.

### 3.2.8 Fourier transform infrared spectroscopy

Infraerd spectra were collected using OMNIC v.9.0 software in connection with a 912A0763 Nicolet iS50 FTIR KBr Gold Spectrometer, which allows for the use of both DRIFT and ATR measurements. A Ge-on-KBr beamsplitter was used. A top-mounted DaTGS mid-IR detector was utilised, capable of IR measurements in the range of 5000 to 100 $cm^{-1}$ . For ATR, the instrument was used as procured, with a monolithic diamond ATR crystal. A 60 psi pressure tower was used to ensure proper contact between the sample and the crystal.

Diffuse Reflectance Fourier Transform Spectra were obtained using FTIR segment of the Nicolet is50. A Harrick Praying Mantis High Temperature Reaction

Chamber with KBr windows were used. A 220V Temperature Controller was used, and automated heating profiles were programmed with an EZ-ZONE Configurator software. The cell and the external parts were cooled by an EHEIM 2217 aquarium pump.

A  $N_2$  flow line was regulated by a mass flow controller allowing up to 30ml/min, before it was split in two lines, where the gas could be directed to either flush the cell or bubbling the  $N_2$  through a pyridine bubbler for in-situ adsorption studies. A nitrogen purge of 30 SCFH was connected directly to the instrument housing to minimize atmospheric disturbances for the IR-beam. An illustration of the set-up can be seen in Figure 3.5

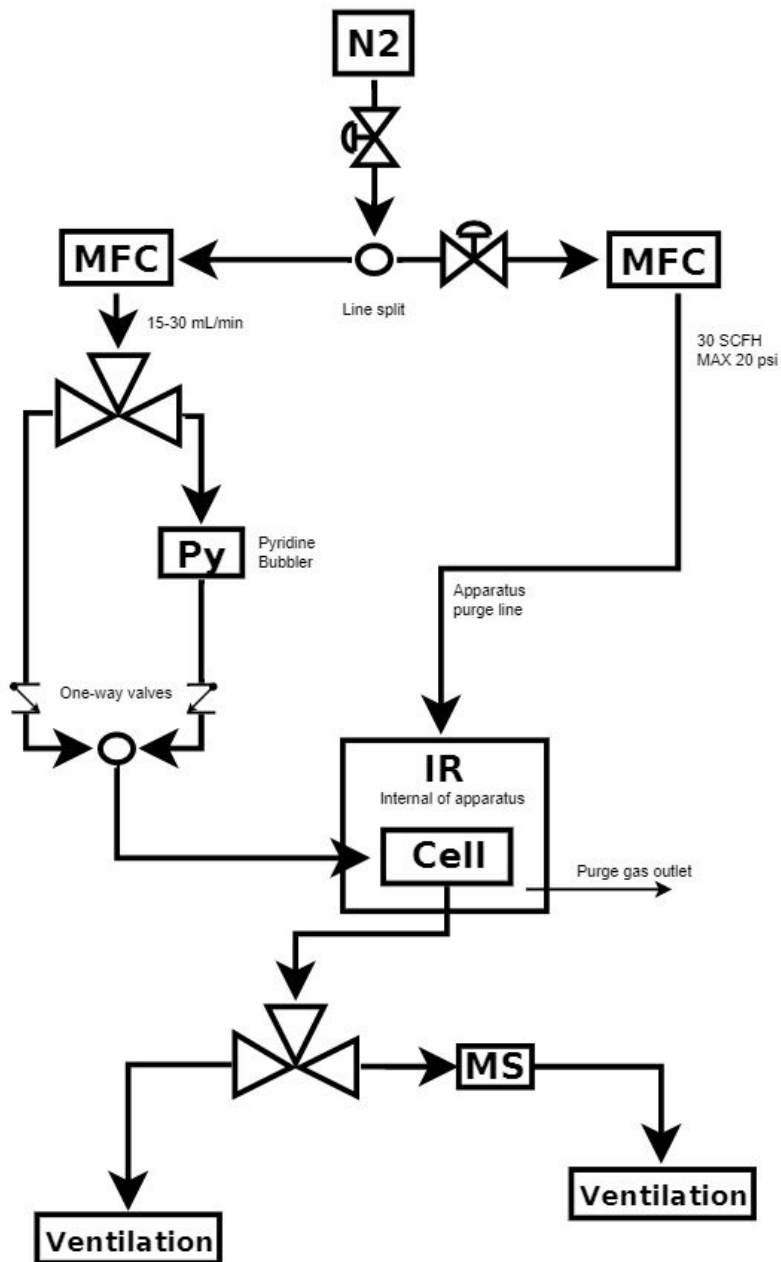


Figure 3.5: Flow sheet of the set-up used for the experiment.

### ATR-FTIR

ATR-FITR was performed for initial investigation of the support, the reference catalyst and both the modified catalysts. For obtaining a background, measurement of an empty sample holder was conducted, before the catalyst sample was placed in the sample holder and pressed to the surface by the pressure tower. 32 scans at a resolution of  $4\text{cm}^{-1}$  was used for scanning, and an absorbance spectrum was calculated by the OMNIC software.

### In-situ DRIFT

In-situ DRIFT with pyridine adsorption was performed for studying the surface structure of the catalyst samples, as well as the change in acidity as a function of added tungsten. The procedure is based on the work of David A. Coucheron[15]. The sample was mixed with KBr to get approximately 1wt% sample, see Table 3.3, as this is required by the instrument for obtaining accurate measurements. The sample mixture was then placed inside the praying mantis cell, and flushed with pure  $N_2$  gas at 15ml/min. During flushing, the sample was heated to 773K at  $50^\circ\text{C/h}$  and held at that temperature for 1h to ensure proper dehydroxylation, before being cooled to 423K.

Pyridine was then introduced for 30 min at a rate of 30mL/min, before flushing with pure  $N_2$  gas at 15mL/min for 1h to ensure the removal of all physisorbed species. During both pyridine introduction and the subsequent flushing, a reflectance spectra was taken each minute. A background was taken right before the introduction of pyridine for each sample.

**Table 3.3:** Weight percentage of the different samples in KBr.

Sample	weight percentage[%]
$\gamma$ -alumina	0.99
Reference catalyst	0.98
Post-modified catalyst	0.99
Pre-modified catalyst	0.98

### Data Analysis

OMNIC v.9.0 was used for data recording and processing for both ATR and in-situ DRIFT measurements with pyridine adsorption. For quantitative interpretation of pyridine adsorption spectra, measured in reflectance units, all spectras were converted to Kubelka-Munk units by the built-in function in OMNIC, using equation 3.1 [14],

$$f(R_\infty) = \frac{(1 - R_\infty)^2}{2R_\infty} \quad (3.1)$$

where  $R_\infty$  represents the reflectance of an infinitely thick layer. Spectras were then peakfitted using FITYK v.0.98 and Voigt peak shape and Levenberg-Marquardt fitting model, based on the work of David A. Coucheron[15], observed peak structure and theoretically expected peaks.

Besides the surface structure of transition aluminaes, Lewis and Brønsted acid sites are of great interest due to their catalytic properties and effect on its supported metals [56, 2, 83, 17]. Unfortunately, only Brønsted acid sites can be observed due to their OH band, while Lewis acid sites have coordinatively unsaturated sites, and are thus not a vibrator. A solution of this problem is the use of a probe molecule consisting of a Lewis base, but not every Lewis base are suitable. The probe has to be small enough to interact with all available sites, and its basic strength should be strong enough to interact to even weak acid sites. However, it should not be so strong that it modifies the structure of the support. One probe molecule that fits these criterias is pyridine, and it has thus been widely investigatet throughout the years [14, 75, 55, 36, 5, 34, 41, 40, 35]. The region around 1600 and 1400 $\text{cm}^{-1}$  is commonly of the greatest interest, as these originate from the 8a and 19b ring vibration in the pyridine, giving the most intensive vibration [36]. Especially frequencies given in Table F.1 in Appendix F are of interest, as the aim of tungsten modification is to increase acidity of the platinum catalyst.



# Chapter 4

## Results

### 4.1 Nitrogen adsorption

Surface area, pore volume and average pore width was obtained from nitrogen adsorption. The results are given in Table 4.1, and BET isotherms can be found in **Appendix something**, together with pore size distribution. As can be seen in Table 4.1, the surface area and pore volume of  $\gamma$ -alumina was measured to be within the range of other studies[12, 73, 31, 68, 39], whereas the addition of platinum had a small or no effect on these parameters. This was also true for modified support.

Surface area of  $\text{WO}_3/\text{ZrO}_2$  seems to be within the medium surface area region compared to values reported in literature[70, 33, 44, 13], with relatively narrow average pore diameter compared to the alumina supported catalysts.

**Table 4.1:** The surface area, pore volume and average pore width of calcined  $\gamma$ -Al<sub>2</sub>O<sub>3</sub>, reference catalyst, as well as post- and pre-modified catalyst, calculated from N<sub>2</sub> adsorption. The calculations of pore size and pore volume are based on BJH desorption method.

Catalyst	BET surface area [m <sup>2</sup> /g]	Pore volume [cm <sup>3</sup> /g]	Avg. Pore Dia. [nm]
$\gamma$ -Al <sub>2</sub> O <sub>4</sub>	146	0.73	144
Pt/Al <sub>2</sub> O <sub>4</sub>	143	0.71	146
Pt-W/Al <sub>2</sub> O <sub>4</sub>	136	0.70	150
W-Pt/Al <sub>2</sub> O <sub>4</sub>	135	0.66	149
WO <sub>3</sub> /ZrO <sub>2</sub>	110	0.18	50
Ru/ $\gamma$ -Al <sub>2</sub> O <sub>4</sub> <sup>a</sup>	200	-	-

<sup>a</sup> Surface area of Ru/ $\gamma$ -Al<sub>2</sub>O<sub>4</sub> was given by Alpha Aeser

## 4.2 Dispersion

Both hydrogen and CO chemisorption were performed for 1wt% Pt/ $\gamma$ -alumina. For hydrogen chemisorption, a H<sub>2</sub>:Pt stoichiometry of 2:1 and a H<sub>2</sub>:Ru of 1 was used, while for CO chemisorption a CO:Pt stoichiometry of 1:1 was used, based on available literature [21, 60]. The dispersion and measured crystal size can be seen in Table 4.2. For modified catalyst, only CO chemisorption was used.

It is believed that due to hydrogen being both weakly and strongly chemisorbed on the metal surface of platinum on alumina [53], the accessible metal surface, and thus the dispersion, should be based on the total amount of hydrogen adsorption, and not only the strongly adsorbed. For carbon monoxide chemisorption, the crystal size and dispersion is based on strongly adsorbed species.

Ruthenium dispersion seems to be best governed/determined by strongly adsorbed hydrogen as reported by X. Wu et.al. [80]. It is difficult to interpretate the results from CO chemisorption as it has been reported that, for Ru/SiO<sub>3</sub>, several CO molecules tends to form bonds with a single surface ruthenium atom, like Ru-(CO)<sub>2</sub> and Ru-(CO)<sub>3</sub> [38]. To complicate even more, other studies have reported bridge bonded CO on ruthenium as well [6]. A H<sub>2</sub>:Ru stoichiometry of 1 is recommended [6].

As one can see in Table 4.2, both of the WO<sub>3</sub> modified catalysts experienced a decrease in dispersion of platinum. For post-modified catalyst, this could be a

**Table 4.2:** The dispersion and crystal size of Pt/Al<sub>2</sub>O<sub>3</sub>, Pt-W/Al<sub>2</sub>O<sub>3</sub>, W-Pt/Al<sub>2</sub>O<sub>3</sub> and Ru/Al<sub>2</sub>O<sub>3</sub> calculated by chemisorption of both CO and hydrogen. Dispersion and crystal size are given for strong adsorption unless stated otherwise.

Catalyst	Analysing gas	Dispersion [%]	Crystallite size [nm]
Pt/Al <sub>2</sub> O <sub>4</sub> <sup>a</sup>	H <sub>2</sub>	64	3.2
Pt/Al <sub>2</sub> O <sub>4</sub>	CO	60	1.9
Pt-W/Al <sub>2</sub> O <sub>4</sub>	CO	52	2.2
W-Pt/Al <sub>2</sub> O <sub>4</sub>	CO	55	2.0
WO <sub>3</sub> /ZrO <sub>2</sub> <sup>b</sup>	-	-	-
Ru/Al <sub>2</sub> O <sub>4</sub>	H <sub>2</sub>	5.9	22
Ru/Al <sub>2</sub> O <sub>4</sub> <sup>c</sup>	H <sub>2</sub>	17	7.7

<sup>a</sup>Total adsorption is used for H<sub>2</sub> measurements

<sup>b</sup>As mentioned in Chapter 3.2.2, no chemisorption takes place on tungsten.

<sup>c</sup>Chemisorption on egg shell pellet.

consequence of heat treatment, both from calcination and from the chemisorption procedure, leading to agglomeration or Ostwald ripening. This is supported by the increase in size of Pt-particles on  $\gamma$ -alumina, as can be seen in Chapter 4.4. Still, this does not explain the decreased dispersion of pre-modified catalyst, where platinum only undergoes one calcination procedure. It is therefore believed that addition of WO<sub>3</sub> blocks the access of CO to platinum, leading to lower dispersion values.

For alumina supported ruthenium, there is a large difference between crushed and uncrushed pellet. This could be a consequence of the grinding procedure, where ruthenium might be covered by alumina from the ruthenium free interior, preventing hydrogen chemisorption.

### 4.3 X-Ray Fluorescence

For obtaining sample composition, X-ray fluorescence was conducted. A summary of catalyst composition can be seen in Table 4.3.

XRF results show that the amount of platinum in the prepared catalyst cor-

**Table 4.3:** Element composition for alumina supported Pt catalyst, non-, post- and premodified, alumina supported Ru catalyst and zirconia supported WO<sub>3</sub> catalyst. Each catalyst were analyzed two times, and the middle values are given. Al<sub>2</sub>O<sub>3</sub> and ZrO<sub>2</sub> have a detection limit of 0.01mm and 1.03mm, respectively.

Catalyst	Element [wt%]	Analyzing depth [mm]
Pt/Al <sub>2</sub> O <sub>3</sub>	1.2wt%PtO <sub>2</sub>	2.79
Pt-WO <sub>3</sub> /Al <sub>2</sub> O <sub>3</sub>	0.8wt%PtO <sub>2</sub>	2.79
	0.7wt%WO <sub>3</sub>	1.96
WO <sub>3</sub> Al <sub>2</sub> O <sub>3</sub> <sup>a</sup>	0.9wt%WO <sub>3</sub>	1.96
WO <sub>3</sub> -Pt/Al <sub>2</sub> O <sub>3</sub> <sup>a</sup>	0.8wt%PtO <sub>2</sub>	2.79
	0.7wt%WO <sub>3</sub>	1.96
Ru/Al <sub>2</sub> O <sub>3</sub> <sup>b</sup>	2wt%Ru	-
WO <sub>3</sub> /ZrO <sub>2</sub>	14wt%WO <sub>3</sub>	1.04
	1.5wt%HfO <sub>2</sub>	1.24
	1.0wt%CeO <sub>2</sub>	0.23

<sup>a</sup>Content of WO<sub>3</sub> after first incipient wetness impregnation step was measured to be 0.8wt%.

<sup>b</sup>Values are given by the Alpha Aeser.

responds to the desired value within a reasonable range. This also shows that there was no detection of impurities due to sample preparation or contamination in neither  $\gamma$ -alumina nor the platinum. There were some contaminations detected in the pellet, but these mainly originated from impurities in the binding material, boric acid. Even though catalyst impurities in the catalyst could be masked by those from the binder, these were left out due to their low wt%. Previous test-measurements have shown the importance and effect of the degree of homogeneity in the sample prepared. As the difference in grain size of binder and sample are not the same, achieving homogenous pellets are difficult. Even with manual grinding, mechanical loss will occur, resulting in lower measured values. Values in Table 4.3 should therefore not be used as absolute, but rather as an indication of the composition.

The importance of homogeneity could arise from the difference in penetration depth for different elements. If the sample accumulates on the surface of the pellet, the instrument would detect a higher amount of Al<sub>2</sub>O<sub>3</sub> with an analyzing depth of only 0.01 mm compared to a more homogenous pellet. This would also be the case for platina, but because of its greater analyzing depth, this would even out as one moves deeper into the pellet were occurrence of sample are more scarce.

Both post- and pre-modified catalyst seems to contain the same amount of both platinum and tungsten, making comparison of post- and pre-modification effects easier in later studies. The decrease in platinum content after post-modification are believed to be partly due to addition of tungsten oxide. This is also believed to be the case for tungsten in pre-modified catalyst after platinum addition.

Comercial WO<sub>3</sub>/ZrO<sub>2</sub> catalyst was found to contain hafnium, a trait commonly found in zircona support, as Hf and Zr shares a number of chemical properties, and is therefore hard to separate [16].

## 4.4 SEM

Scanning electron microscopy (SEM) analysis was carried out to investigate the surface topography.

As seen from Figure 4.1(a), using BSE, there exists a high number of particles with a diameter of 50-70nm on the surface. Nevertheless, not all alumina spheres have such a high density of small particles, but rather fewer and larger ones, with a diameter of 120-130nm, as seen in Figure 4.1(b). This shows that it might

be some difficulties with homogeneous dispersion of platinum on the alumina support.

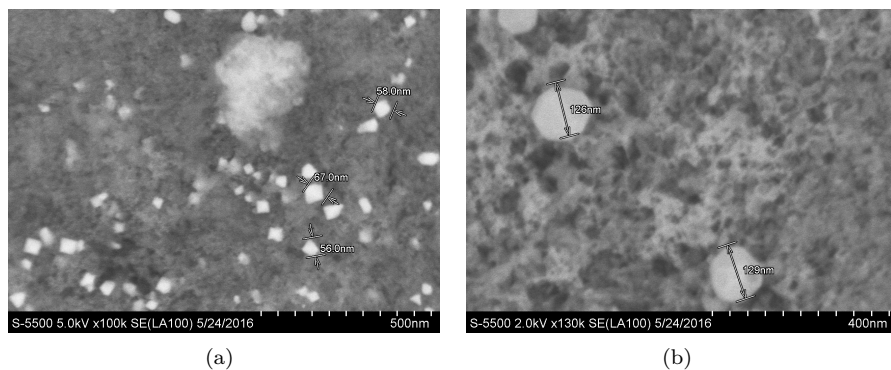


**Figure 4.1:** ??Platinum catalyst with high amount of small surface particles and 4.1(b) with smaller amount of large surface particles.

Due to chemisorption giving a crystallite size of approximately 2nm, and that the average pore volume diameter, given by BET, of 14nm, it is believed that particles of this size only occur on the surface of the support.

This is also supported by the fact that large particles within the alumina structure would certainly block pores, resulting in decreased surface area. As reported in Chapter 4.1, no such decrease in surface were observed.

For Post modified catalyst, surface particles seem to be slightly larger, a feature belived to be caused by sintering of Pt particles during the second calcination, see Figure 4.2(a) and 4.2(b).

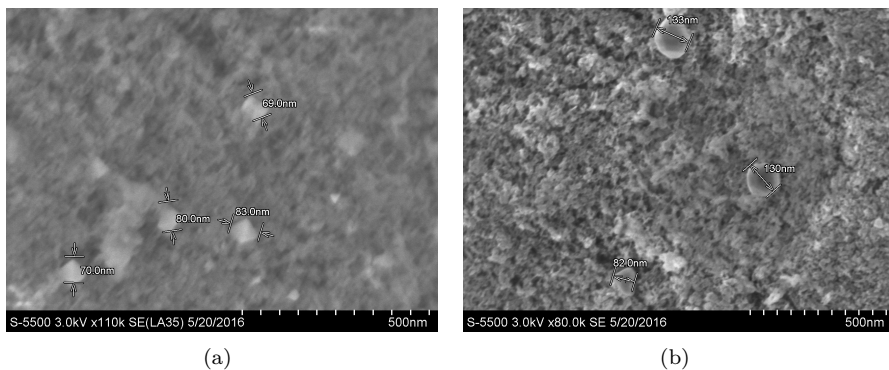


**Figure 4.2:** 4.2(a) Post-modified catalyst with high amount of small surface particles and 4.2(b) with smaller amount of large surface particles.

For pre-modified catalyst, size of surface particles were even greater than those of post-modified catalyst, as well as having a variety of different sizes, as seen in Figure 4.3(a) and 4.3(b). This indicates that calcination is not the largest contributor, but only plays a small role in particle growth. As the size is larger after both post- and pre-modification, it would be reasonable to ascribe this trait to tungsten oxide.

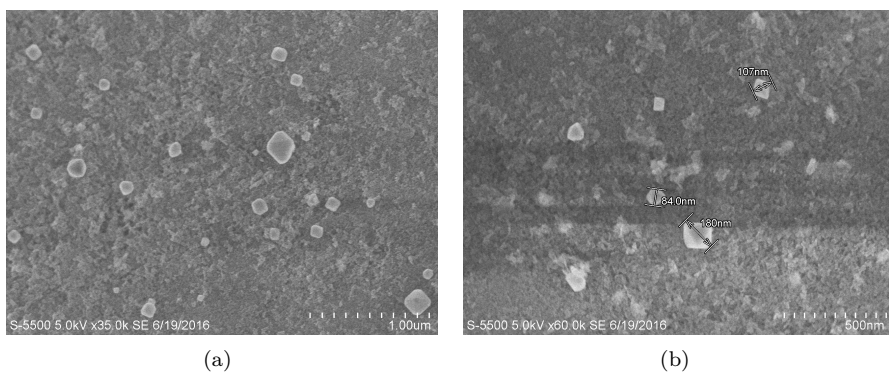


**Figure 4.3:** 4.3(a) Particle size on pre-modified catalyst with and 4.3(b) a variety of particles of different size.

As mentioned in Chapter 1.1, larger particles of platinum have showed resistance towards deactivation than smaller particles, due oxygen forming stronger bonds with smaller Pt-particles. Even though the surface particles only make up a small amount of the total platinum, this could help increase activity during NO oxidation due to resistance towards self-inhibition[63].

### EDX measurements

EDX was carried out for element analysis and shows that the surface particles in platina catalyst consist mainly of platinum in its elemental form. EDX images of both post- and pre-modified also shows that surface particles consist mainly of elemental platinum, with small amounts of tungsten oxide.

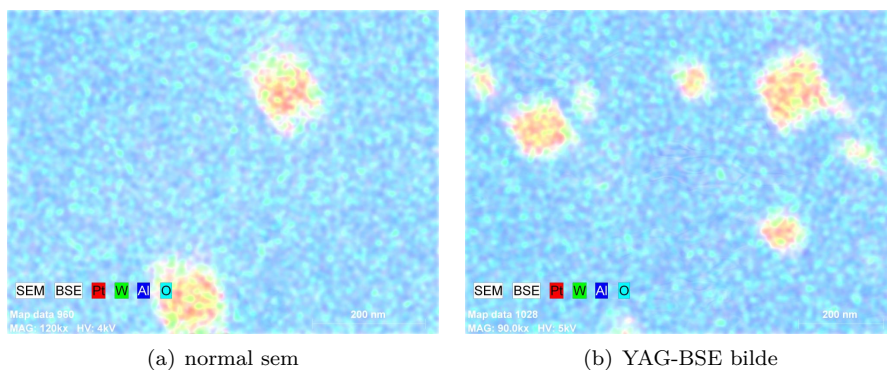


**Figure 4.4:** Composition of particles on 4.4(a) post-modified catalyst and 4.4(b) pre-modified catalyst. As can be seen, particles consists mainly of platinum with small amounts of tungsten.

EDX imaging was also done for crushed post-modified catalyst to see metal distribution within the interior of the support. From Figure 4.5(a) and 4.5(b), it seems that both Pt and WO<sub>3</sub> is well dispersed without large particle formations within each alumina sphere. This is also the case pre-modified catalyst, as seen in Figure 4.5(c) and 4.5(d).



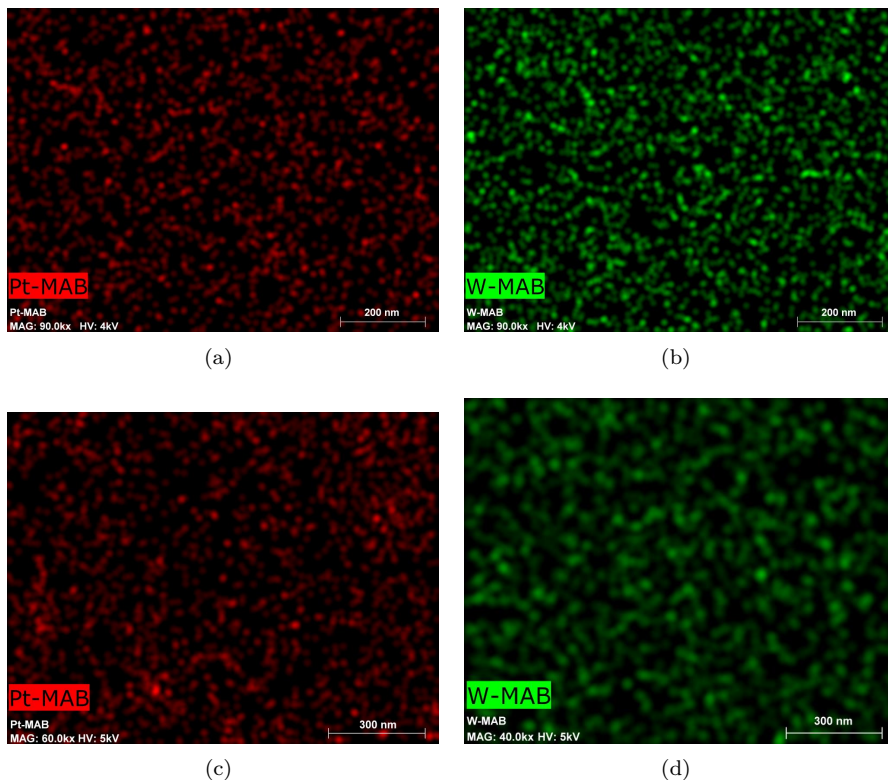


**Figure 4.5:** 4.5(a) The distribution of platinum and 4.5(b) tungsten in the interior structure of crushed post-modified catalyst. 4.5(c) The distribution of platinum and 4.5(d) tungsten particles in pre-modified catalyst.

## 4.5 X-ray diffraction

Figure 4.6 shows the XRD profiles of  $\gamma$ - $\text{Al}_2\text{O}_3$ ,  $\text{Pt-Al}_2\text{O}_3$ ,  $\text{Pt-W-Al}_2\text{O}_3$  and  $\text{W-Pt-Al}_2\text{O}_3$ . The crystalline phases of the samples are matched to reference patterns/characteristic spinel reflections (vertical lines), using “Diffrac. Eva V4.1”.

The XRD patterns of  $\eta$  and  $\gamma$ -alumina, seen in Figure E.1, Appendix E, are

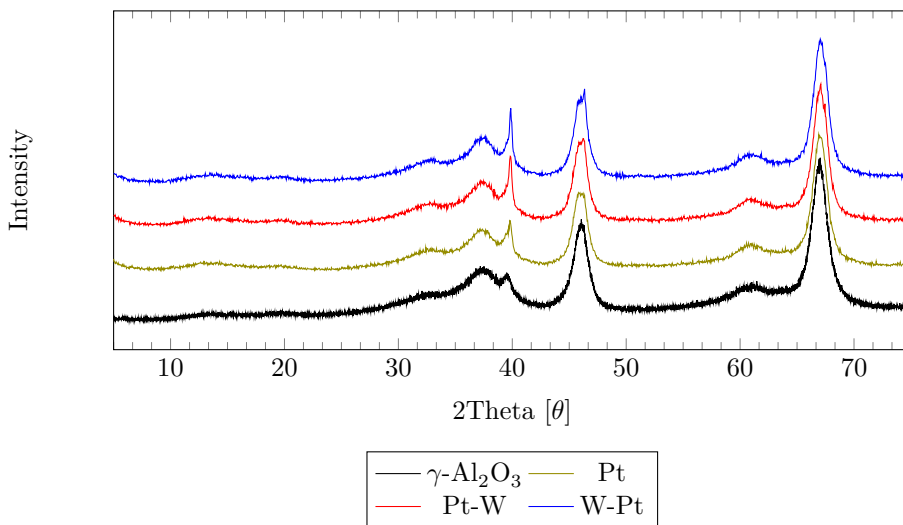


**Figure 4.6:** XRD profile of  $\gamma$ -Al<sub>2</sub>O<sub>3</sub>, Pt-Al<sub>2</sub>O<sub>3</sub>, Pt-W-Al<sub>2</sub>O<sub>3</sub> and W-Pt-Al<sub>2</sub>O<sub>3</sub>.

almost identical, with only a slightly difference in the width of some peaks, mainly due to the occupancy of the sites by cations and vacancies, more than any structural differences. In respect to this, most authors suppose that the two transition phases are essentially the same. Even so, it has been suggested that  $\eta$ -alumina has stronger Lewis acid sites and therefore a slightly higher activity than  $\gamma$ -alumina [31].

Still, the peaks are notable broad compared to other crystalline compounds, as expected from alumina. Owing to alumina being highly amorphous, assignment of phase type or calculation of crystallite size is for this reason rather challenging [34] | According to Guido Busca [31], this is a result from structural disorder within the cubic structure of alumina.

As for the reference catalyst containing 1wt% Pt and the modified catalysts, a small elevation in the peak around 40  $\theta^\circ$  region is observed, together with a broadening of the peak at the 40  $\theta^\circ$  region, see Figure 4.6. No change in morphology should arise by means of calcination procedure alone, as calcination of pure alumina occurred at a higher temperature. It is therefore believed that these alterations stem from platinum and tungsten crystallites.

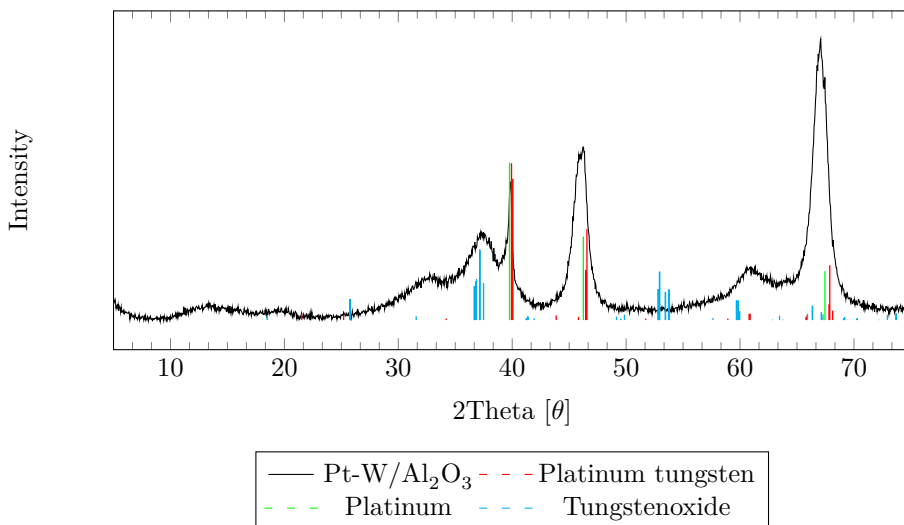


**Figure 4.7:** XRD profile of Pt-W/ $\text{Al}_2\text{O}_3$  and its corresponding spinel reflections.

From figure 4.7 it can be seen that the spinel reflections for platinum is overlapping with that of aluminum. Unfortunately, this seems to be the case for Tungsten as well, making it impossible to ascribe phase or calculate crystallite size for neither of the compounds. It must be noted that the height of spinel reflections do not necessarily reflect the measured intensity.

In addition to overlapping peaks, the small changes in the diffraction pattern could be a consequence of either a weight percentage or crystallite sizes of metals below or close to detection limit, which have been reported to be the case for  $\text{WO}_3$ [83].

Profiles matching characteristic spinel reflections for individual samples can be seen in Figure E.1, E.2, E.3 and E.4 found in Appendix E.

## 4.6 Temperature Programmed Reduction

Temperature Programmed Reduction was performed for Pt- $\text{Al}_2\text{O}_3$  to find optimal reduction temperature. No hydrogen uptake were detected seen, as shown

in Figure 4.8.

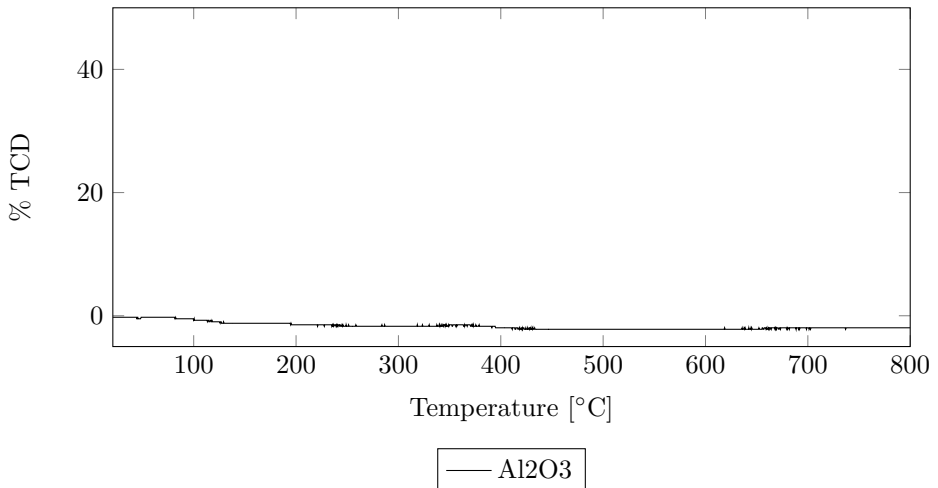


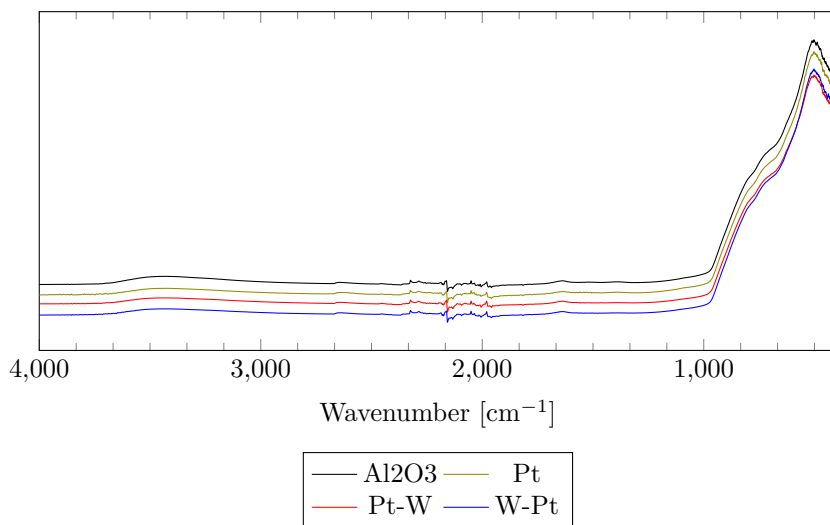
**Figure 4.8:** TPR of Pt/Al<sub>2</sub>O<sub>3</sub> from ambient temperature to 800°C.

The lack of hydrogen uptake could be caused by the fact that platinum is already in a reduced state. Ivanova et al.[29] have reported that in H<sub>2</sub>-TPR studies of platinum and paladium supported on alumina, platina was reduced already at 44°C. In the same study, it was found that reduction temperature for Pd catalyst depended on the calcination temperature, theorized to be caused by a decrease in Pd and Al<sub>2</sub>O<sub>3</sub> interactions. As platinum and paladium are both elements of the same group, this could also be true for platinum. Additionally, Rossin[62] discovered that by increased calcination temperature of alumina supported platinum catalyst led to an increase in the extent of platinum reduction. This implies that the catalyst is in an already reduced state, caused either during the leak test sequence, or by calcination at 600°C. It would therefore be of interest to performe H<sub>2</sub>-TPR at a lower temperature.

## 4.7 Fourier Transform Infrared Spectroscopy

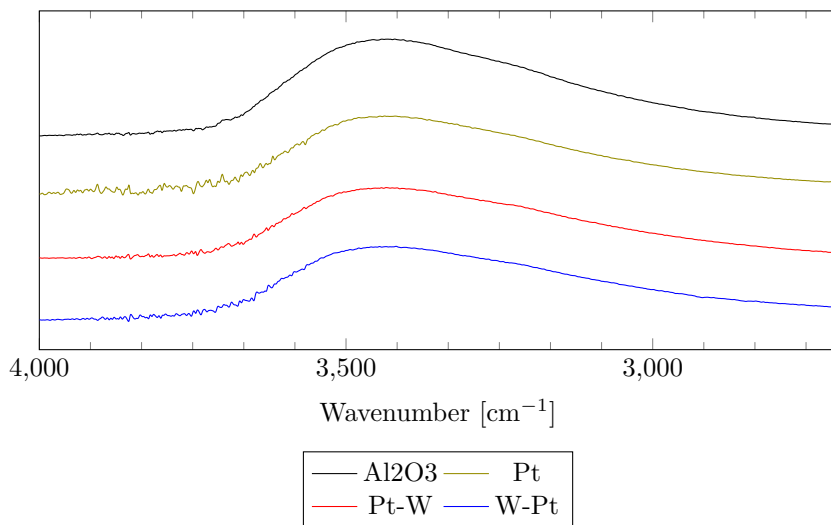
### 4.7.1 FTIR-ATR

ATR investigation was conducted to detect the changes in the surface structure of the catalyst to confirm the presence of modifier.



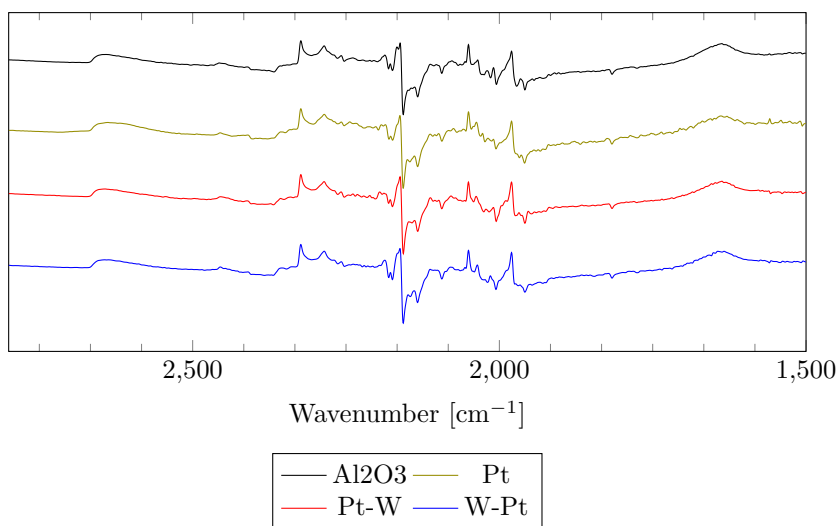
**Figure 4.9:** ATR absorbance-spectra of Al<sub>2</sub>O<sub>3</sub>, Pt/Al<sub>2</sub>O<sub>3</sub>, Pt-W/Al<sub>2</sub>O<sub>3</sub> and W-Pt/Al<sub>2</sub>O<sub>3</sub> in the mid IR region. Y-axis is given in arbitrary units.

Figure 4.9 compares the mid-range spectral region of  $\gamma$ -alumina, reference catalyst, post and pre-modified catalysts. It has been reported that the addition of Tungsten to alumina increases its acidity by an increased amount of Brønsted and Lewis acid sites [83]. It will therefore be natural to investigate the OH region at 3000-3600cm<sup>-1</sup>, as Brønsted-acid sites are usually identified through the  $\nu(\text{OH})$  band of hydroxyl groups [76]. For comparison purposes, other wavenumbers have also been investigated closer. As seen from Figure 4.10, it appears to be no significant changes in these regions due to modification. This is also the case for Figure 4.11 and 4.12 indicating that the modification does not alter the hydroxyl group, nor any other region within the mid-range spectra. Vibrations of metal oxygen bonds on the surface are not visible in the observable spectra, as



**Figure 4.10:** ATR absorbance-spectra of Al<sub>2</sub>O<sub>3</sub>, Pt/Al<sub>2</sub>O<sub>3</sub>, Pt-W/Al<sub>2</sub>O<sub>3</sub> and W-Pt/Al<sub>2</sub>O<sub>3</sub> in the OH region between 4000-3500 cm<sup>-1</sup>. Y-axis is given in arbitrary units.

exists in the same spectral region as lattice vibrations. For metal-metal bonds, the vibrational frequencies lie beyond that of conventional FTIR spectrometers [5]. Changes due to metal addition on the surface will therefore not lead to any changes in the IR spectra by itself, unless other surface groups are altered, or a probe molecule is introduced.



**Figure 4.11:** ATR absorbance-spectra of Al<sub>2</sub>O<sub>3</sub>, Pt/Al<sub>2</sub>O<sub>3</sub>, Pt-W/Al<sub>2</sub>O<sub>3</sub> and W-Pt/Al<sub>2</sub>O<sub>3</sub> in the 2750-1500cm<sup>-1</sup> region. Y-axis is given in arbitrary units.

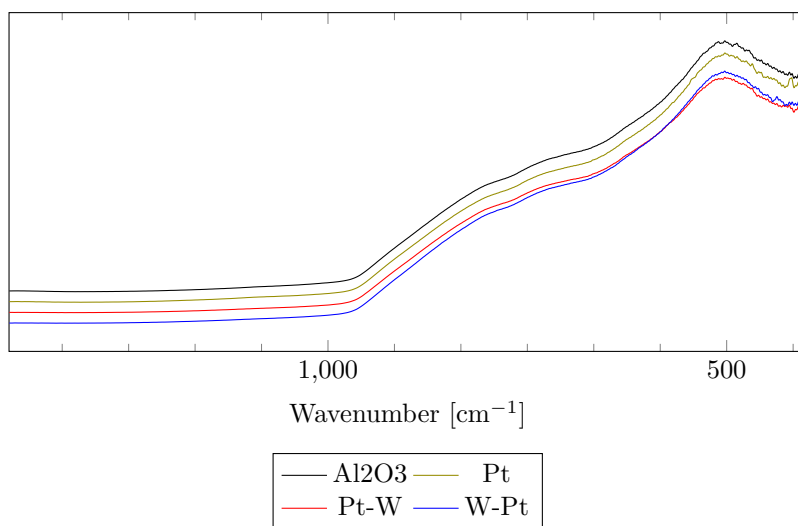
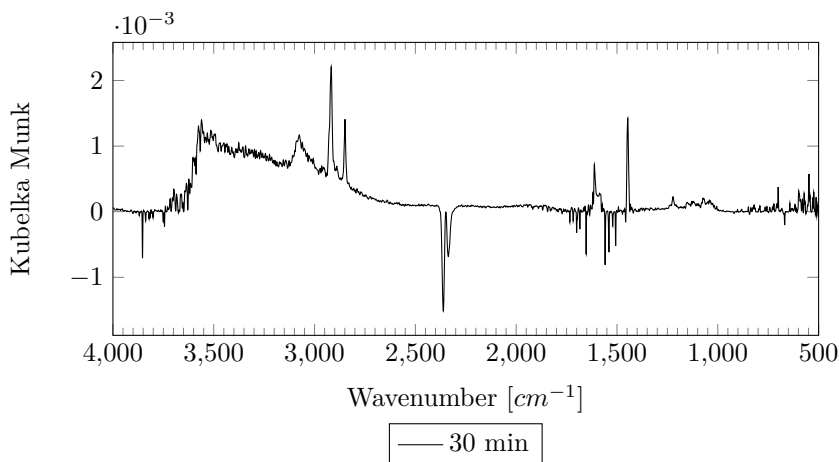


**Figure 4.12:** ATR absorbance-spectra of Al<sub>2</sub>O<sub>3</sub>, Pt/Al<sub>2</sub>O<sub>3</sub>, Pt-W/Al<sub>2</sub>O<sub>3</sub> and W-Pt/Al<sub>2</sub>O<sub>3</sub> in the 1500-400cm<sup>-1</sup> region. Y-axis is given in arbitrary units.



## 4.7.2 DRIFTs

In-situ DRIFT was used to further investigate the effect of catalyst modification by pyridine adsorption. The use of pyridine as a probe molecule in adsorption on  $\gamma$ -alumina has been widely investigated throughout the years [14, 75, 55, 36, 5, 34, 41, 40, 35].



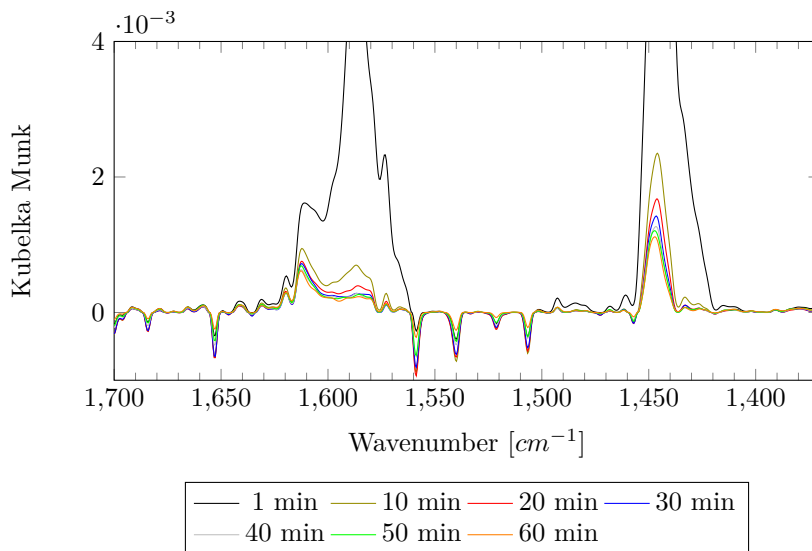
**Figure 4.13:** DRIFTIR-spectrum of  $\gamma$ -Al<sub>2</sub>O<sub>3</sub> in the region of 4000-500cm<sup>-1</sup> 30 min after bubbling of pyridine was ended. The spectra were taken at 150 °C under a flow of 15 mL min<sup>-1</sup> N<sub>2</sub>.

Figure 4.13 shows the Kubelka-Munk spectrum of pyridine adsorbed on  $\gamma$ -alumina 30min after ended exposure. The bands at 1600 and 1400 cm<sup>-1</sup> represent the 8a and 8b and the 19a, and 19b ring vibrations of pyridine, respectively. The bands at 2350 cm<sup>-1</sup> represent the CO<sub>2</sub> region, the bands at 3100-2700 cm<sup>-1</sup> represent the CH-stretch region while the broad band around 3500 cm<sup>-1</sup> represents the hydroxyl area.

For this thesis, only known bands originated from pyridine adsorption are of interest, and negative bands in the area of 1800-1350cm<sup>-1</sup> have therefore not been discussed.

Ring vibrations in pyridine are known for giving the most intensive vibration for pyridine adsorption[36, 47], and will therefore be more closely investigated. For this purpose, a Kulba Munk spectrum in the 1400 and 1600 cm<sup>-1</sup> region for pyridine adsorbed at  $\gamma$ -alumina was plotted, comparing the pyridine adsorption

every 10 min after ended exposure. This can be seen in Figure 4.14. For comparison reasons, the spectra of pyridine adsorbed on pure alumina is left out, as its high intensity compared to those of Pt/ceAl<sub>2</sub>O<sub>3</sub>, Pt-ceWO<sub>3</sub>/ceAl<sub>2</sub>O<sub>3</sub> and ceWO<sub>3</sub>-Pt/ceAl<sub>2</sub>O<sub>3</sub>.



**Figure 4.14:** IR-spectrum of  $\gamma$ -Al<sub>2</sub>O<sub>3</sub> in the wavenumber range of 1350-1700cm<sup>-1</sup> for every 10 min after bubbling of pyridine was ended. The spectra were taken at 150 °C under a flow of 15 mL min<sup>-1</sup> N<sub>2</sub>.

As seen from the figure, pyridine desorbs quickly after bubbling stops, with a decrease in intensity for all bands. After approximately 30-40 minutes, the signal seems to stabilize, as physisorbed pyridine is removed from the surface. During this removal, strongly hydrogen-bonded pyridine seems to gradually disappear, while coordinated bound pyridine remains relatively stable, demonstrated by the rapid decrease at the 1588cm<sup>-1</sup> band compared the 1612cm<sup>-1</sup> bands, respectively[40]. For the 19a and 19b ring vibration region, the band seems to shift from weakly coordinated bands at 1444cm<sup>-1</sup> and weak hydrogen bands in the favor of very strong coordinately bonds at 1447 [40, 34], as expected.

As seen by Figure 4.15, the band at 1612 and 1588, associated with medium Lewis acid and strong hydrogen bonds[40], are significantly weaker in Platinum

catalyst compared to tungsten modified catalyst, showing an increase in medium Lewis acid sites after modification.

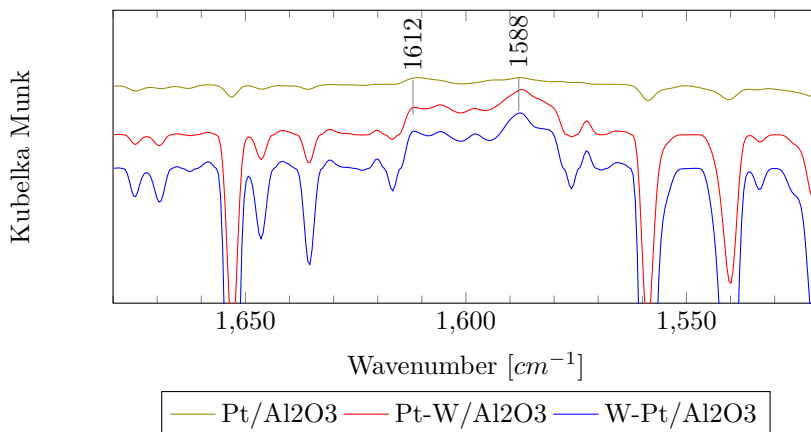


**Figure 4.15:** IR-spectrum of Pt/ $\text{Al}_2\text{O}_3$ , Pt-W/ $\text{Al}_2\text{O}_3$  and W-Pt/ $\text{Al}_2\text{O}_3$  in the wavenumber range of 1700-1500  $\text{cm}^{-1}$  for 30 min after bubbling of pyridine was ended. The spectra were taken at 150  $^\circ\text{C}$  under a flow of 15  $\text{mL min}^{-1}$   $\text{N}_2$ . For both spectras, an y-offset is introduced for easier interpretation. Y-axis is given in arbitrary units.

From the 19a, and 19b vibration area, see Figure 4.16, a strongly coordinated band at 1450  $\text{cm}^{-1}$  and strong hydrogen bond at 1444 can be observed for modified catalyst. At comparison with platina catalyst, both of these bands seem to have red shift, indicating weaker bond strength of these sites [23, 75].

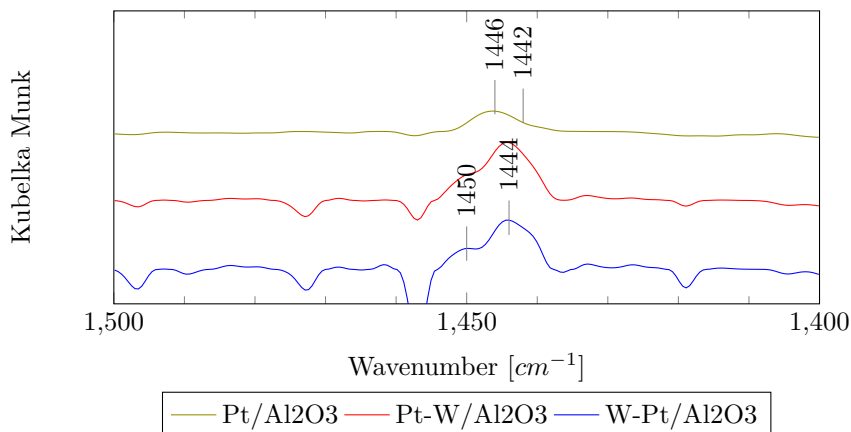


**Figure 4.16:** IR-spectrum of Pt/Al<sub>2</sub>O<sub>3</sub>, Pt-W/Al<sub>2</sub>O<sub>3</sub> and W-Pt/Al<sub>2</sub>O<sub>3</sub> in the wavenumber range of 1500-1420 cm<sup>-1</sup> for 30 min after bubbling of pyridine was ended. The spectra were taken at 150 °C under a flow of 15 mL min<sup>-1</sup> N<sub>2</sub>. For both spectras, an y-offset is introduced for easier interpretation. Y-axis is given in arbitrary units.

In general, bands associated with both medium and strong acidic sites are barely present in platinum containing catalyst, indicating that little pyridine adsorbs on the surface. Beard and Zhang found that highly dispersed platinum particles behave as bases when interacting with acidic alumina, thus resulting in decreased adsorption of pyridine [3]. This could explain the reduced intensity for platinum catalyst. As mentioned in Chapter 4.2, average crystallite size of platinum has been measured to be around 1.8nm, only slightly larger than what have been reported. The addition of WO<sub>3</sub> have been reported to increase both the number of Lewis and Brønste acids[83] in alumina. This could explain the increased intensity associated with Lewis acids, indicating that tungsten counteracts the basic properties of platinum particles.

As pyridine might perturb the hydroxyl groups of alumina, this area was also investigated, shown by Figure 4.17(a). It has been found that increased intensity of bands at 3561 and 3512 cm<sup>-1</sup> suggest formation of hydrogen bonds, while negative bands in the area between 3800-3650 cm<sup>-1</sup> are caused by the perturbation of OH groups [41, 37]. When pyridine interacts with Lewis acids of different strength, the electron density within the pyridine ring structure changes. As pyridine adsorbs on the surface, this gives rise to hydrogen bonding of different

strength with adjunct OH groups. Ideally, one should therefore be able to correlate band strength from the pyridine adsorption area to those from the OH area, and thus also find the distribution of Lewis acids with different strength [40]. However, this area suffers from a low signal to noise ratio, making it difficult to interpret bands and acid site distribution. The use of pyridine CH stretch region has also been proposed for the same purpose [72], but also here, signal to noise ratio is too low to obtain useful information, as seen in Figure 4.17(b). This area is also associated with risk of contamination from other hydrocarbons, and was therefore not given much attention.

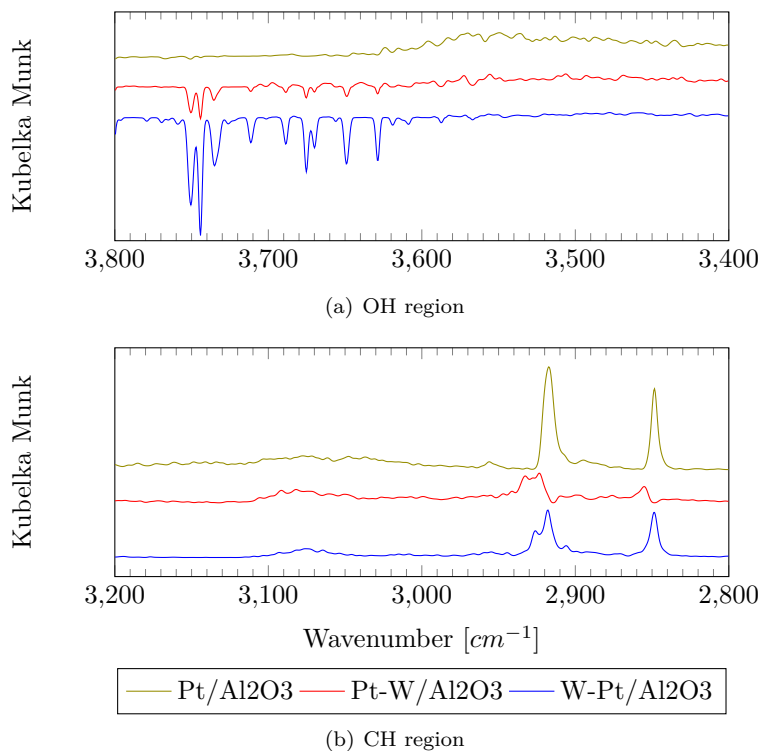


**Figure 4.17:** DRIFTIR-spectrum of Pt/Al<sub>2</sub>O<sub>3</sub>, Pt-W/Al<sub>2</sub>O<sub>3</sub> and W-Pt/Al<sub>2</sub>O<sub>3</sub> in 4.17(a) the OH region and 4.17(b) the CH region 30 min after bubbling of pyridine was ended. The spectra were taken at 150 °C under a flow of 15 mL min<sup>-1</sup> N<sub>2</sub>. For both spectra, a y-offset is introduced for easier interpretation. Y-axis is given in arbitrary units.

# Chapter 5

## Conclusion

This research work focused on the synthesis and characterization of a potential and efficient alumina supported platinum catalyst for achieving NO/NO<sub>2</sub> equilibrium.

The aim of this work was to investigate the properties of alumina supported Pt catalyst both before and after post- and pre-modification with WO<sub>3</sub>. Catalyst with 1%Pt was prepared by aqueous incipient wetness impregnation. Modification with 1.3%WO<sub>3</sub> was carried out by two methods; post-modification with aqueous impregnation of Pt/Al<sub>2</sub>O<sub>3</sub>, and pre-modification with a two-step aqueous impregnation of  $\gamma$ -Al<sub>2</sub>O<sub>3</sub>, first with tungsten, then with platinum.

Nitrogen adsorption showed a surface area of approximately 145m<sup>2</sup>/g. Addition of platinum and tungsten oxide did not alter the surface area, pore volume or pore diameter of the support significantly.

Chemisorption showed that Pt is well dispersed on alumina, with crystallite size of approximately 2nm. It was also discovered a slight decrease in dispersion of Pt for modified catalyst compared to Pt/Al<sub>2</sub>O<sub>3</sub> catalyst. As this occurs for both pre- and post- modified catalyst, but slightly more for post-modification, it is believed that WO<sub>3</sub> blocks access of CO and H<sub>2</sub>. Ruthenium, on the other hand, showed little dispersion with larger crystallite size.

SEM shows the formation of large particles on the surface of alumina spheres. For post-modified catalyst, these particles were slightly larger, while pre-modified catalyst showed a greater variety of size distribution. It is therefore believed that tungsten addition affects the size of these particles. This could also explain

the decrease in dispersion.

An X-ray fluorescence measurement indicates catalysts content of 1.2wt% Pt. In modified catalyst, content of platinum oxide and tungsten oxide were 0.8wt% and 0.7wt% respectively. These values should not be seen as absolute, but rather as an indication of the composition. No impurities were detected in any of prepared catalysts.

No hydrogen uptake were detected by TPR, indicating that platinum is already reduced. Due to the low metal content and alumina being highly amorphous, assignment of phase type or calculation of crystallite size with XRD was not possible.

Ex-situ investigation with ATR could not detect changes in the surface structure as expected. In-situ DRIFT shows that bands at 1446 and 1612  $\text{cm}^{-1}$ , associated with strong and medium Lewis acid sites, are barely present in Pt/ $\text{Al}_2\text{O}_3$ , indicating the lack of acidity. After addition of tungsten, band intensity increased, with a blue shift of the 1446 band to 1450 $\text{cm}^{-1}$ , demonstrating increased acidic strength due to  $\text{WO}_3$ . For all catalysts, no Brønsted acidic sites were found.



## Chapter 6

### Further work

More modified Pt/Al<sub>2</sub>O<sub>3</sub> catalyst with different loading of WO<sub>3</sub> should be prepared in order to verify the increased acidity. TEM imaging of the catalysts should also be conducted in order to verify the platinum and tungsten oxide particle size. XPS would also be of interest, as it can measure the chemical and electronic state of platinum and tungsten oxide. An obvious next step would be to test the catalytic activity, selectivity and stability for NO oxidation to NO<sub>2</sub> at different for each of the catalysts.

After catalytic measurements, it would also be interesting to compare with Pt catalyst on different supports.



# Bibliography

- [1] Handbook of instrumental techniques for analytical chemistry. *Journal of Liquid Chromatography & Related Technologies*, 21(19):3072–3076, 1998.
- [2] Xavier P. Auvray and Louise Olsson. Effect of enhanced support acidity on the sulfate storage and the activity of pt/ $\gamma$ -al<sub>2</sub>o<sub>3</sub> for no oxidation and propylene oxidation. *Catalysis Letters*, 144(1):22–31, 2014.
- [3] BC Beard and ZC Zhang. Probe molecule acid-base characterization of a novel pt/al<sub>2</sub>o<sub>3</sub> hydrodechlorination catalyst. *Catalysis letters*, 82(1-2):1–5, 2002.
- [4] L. Bednářová. *Study of Supported Pt-Sn Catalysts for Propane Dehydrogenation*. PhD thesis, Norwegian University of Science and Technology, Department of Chemical Engineering, 2002.
- [5] Olga B Belskaya, Alexander V Lavrenov, Irina G Danilova, Maxim O Kazakov, Roman M Mironenko, and Vladimir A Likholobov. *FTIR Spectroscopy of adsorbed probe molecules for analyzing the surface properties of supported Pt (Pd) catalysts*. INTECH Open Access Publisher, 2012.
- [6] R.A.Dalla Betta. Measurement of ruthenium metal surface area by chemisorption. *Journal of Catalysis*, 34(1):57 – 60, 1974.
- [7] Divesh Bhatia, Robert W McCabe, Michael P Harold, and Vemuri Balakotaiah. Experimental and kinetic study of no oxidation on model pt catalysts. *Journal of Catalysis*, 266(1):106–119, 2009.
- [8] Alexey Boubnov, Søren Dahl, Erik Johnson, Anna Puig Molina, Søren Bredmose Simonsen, Fernando Morales Cano, Stig Helveg, Lived J Lemus-Yegres, and Jan-Dierk Grunwaldt. Structure–activity relationships

- of pt/al 2 o 3 catalysts for co and no oxidation at diesel exhaust conditions. *Applied Catalysis B: Environmental*, 126:315–325, 2012.
- [9] A Chaloulakou, I Mavroidis, and I Gavriil. Compliance with the annual no 2 air quality standard in athens. required nox levels and expected health implications. *Atmospheric Environment*, 42(3):454–465, 2008.
- [10] J-R Chang, S-L Chang, and T-B Lin.  $\gamma$ -alumina-supported pt catalysts for aromatics reduction: a structural investigation of sulfur poisoning catalyst deactivation. *Journal of Catalysis*, 169(1):338–346, 1997.
- [11] I. Chorkendorff and J. W. Niemantsverdriet. *Catalyst Characterization*, pages 129–166. Wiley-VCH Verlag GmbH Co. KGaA, 2005.
- [12] I. Chorkendorff and J. W. Niemantsverdriet. *Solid Catalysts*, pages 167–214. Wiley-VCH Verlag GmbH Co. KGaA, 2005.
- [13] GK Chuah and S Jaenicke. The preparation of high surface area zirconia—influence of precipitating agent and digestion. *Applied Catalysis A: General*, 163(1):261–273, 1997.
- [14] N.B. Colthup, L.H. Daly, and S.E. Wiberley. *Introduction to Infrared and Raman Spectroscopy*. Elsevier Science, 1990.
- [15] David A. Coucheron. In-situ ftir studies of surface modified fischer-tropsch catalysts. Technical report.
- [16] CE Curtis, LM Doney, and JR Johnson. Some properties of hafnium oxide, hafnium silicate, calcium hafnate, and hafnium carbide. *Journal of the American Ceramic Society*, 37(10):458–465, 1954.
- [17] Jazaer Dawody, Magnus Skoglundh, and Erik Fridell. The effect of metal oxide additives (wo 3, moo 3, v 2 o 5, ga 2 o 3) on the oxidation of no and so 2 over pt/al 2 o 3 and pt/bao/al 2 o 3 catalysts. *Journal of Molecular Catalysis A: Chemical*, 209(1):215–225, 2004.
- [18] Joel Despres, Martin Elsener, Manfred Koebel, Oliver Kröcher, Bernhard Schnyder, and Alexander Wokaun. Catalytic oxidation of nitrogen monoxide over pt/sio 2. *Applied Catalysis B: Environmental*, 50(2):73–82, 2004.
- [19] M. Fadoni and L. Lucarelli. Temperature programmed desorption, reduction, oxidation and flow chemisorption for the characterisation of heterogeneous catalysts. theoretical aspects, instrumentation and applications. In A. Dabrowski, editor, *Adsorption and its Applications in Industry and*

- Environmental Protection Vol.I: Applications in Industry*, volume 120, Part A of *Studies in Surface Science and Catalysis*, pages 177 – 225. Elsevier, 1999.
- [20] RJ Farrauto and RM Heck. Environmental catalysis into the 21st century. *Catalysis Today*, 55(1):179–187, 2000.
- [21] John Freel. Chemisorption on supported platinum: Ii. stoichiometry for hydrogen, oxygen and carbon monoxide. *Journal of Catalysis*, 25(1):149–160, 1972.
- [22] J Friebel and RFW Köpsel. The fate of nitrogen during pyrolysis of german low rank coals—a parameter study. *Fuel*, 78(8):923–932, 1999.
- [23] NS Gill, R Hi Nuttall, DE Scaife, and DW Ao Sharp. The infra-red spectra of pyridine complexes and pyridinium salts. *Journal of Inorganic and Nuclear Chemistry*, 18:79–87, 1961.
- [24] MA Gómez-García, V Pitchon, and A Kiennemann. Pollution by nitrogen oxides: an approach to no x abatement by using sorbing catalytic materials. *Environment international*, 31(3):445–467, 2005.
- [25] FJ Gracia, JT Miller, AJ Kropf, and EE Wolf. Kinetics, ftir, and controlled atmosphere exafs study of the effect of chlorine on pt-supported catalysts during oxidation reactions. *Journal of Catalysis*, 209(2):341–354, 2002.
- [26] Jerzy Haber, Jochen H Block, and Bernard Delmon. Methods and procedures for catalyst characterization. *Handbook of Heterogeneous Catalysis*, 2008.
- [27] Chin-Pei Hwang and Chuin-Tih Yeh. Platinum-oxide species formed by oxidation of platinum crystallites supported on alumina. *Journal of Molecular Catalysis A: Chemical*, 112(2):295–302, 1996.
- [28] Akiko Ishikawa, Shin'ichi Komai, Atsushi Satsuma, Tadashi Hattori, and Yuichi Murakami. Solid superacid as the support of a platinum catalyst for low-temperature catalytic combustion. *Applied Catalysis A: General*, 110(1):61–66, 1994.
- [29] AS Ivanova, EM Slavinskaya, RV Gulyaev, VI Zaikovskii, Stonkus, IG Danilova, LM Plyasova, IA Polukhina, and AI Boronin. Metal-support interactions in pt/al 2 o 3 and pd/al 2 o 3 catalysts for co oxidation. *Applied Catalysis B: Environmental*, 97(1):57–71, 2010.

- [30] M Tayyeb Javed, Naseem Irfan, and BM Gibbs. Control of combustion-generated nitrogen oxides by selective non-catalytic reduction. *Journal of Environmental Management*, 83(3):251–289, 2007.
- [31] F.C. Jentoft. *Advances in Catalysis*. Number v. 57 in *Advances in Catalysis*. Elsevier Science, 2014.
- [32] Vladimir Karpenko. Some notes on the early history of nitric acid: 1300-1700. *Bulletin for the History of Chemistry*, 34(2):105, 2009.
- [33] Dalibor Kaucký, Blanka Wichterlová, Jiri Dedecek, Zdenek Sobalik, and Ivo Jakubec. Effect of the particle size and surface area of tungstated zirconia on the wo x nuclearity and n-heptane isomerization over pt/wo 3-zro 2. *Applied Catalysis A: General*, 397(1):82–93, 2011.
- [34] Abbas A Khaleel and Kenneth J Klabunde. Characterization of aerogel prepared high-surface-area alumina: In situ ftir study of dehydroxylation and pyridine adsorption. *Chemistry–A European Journal*, 8(17):3991–3998, 2002.
- [35] Tomoyuki Kitano, Tomohiro Hayashi, Toshio Uesaka, Tetsuya Shishido, Kentaro Teramura, and Tsunehiro Tanaka. Effect of high-temperature calcination on the generation of brønsted acid sites on wo3/al2o3. *Chem-CatChem*, 6(7):2011–2020, 2014.
- [36] Charles H. Kline and John Turkevich. The vibrational spectrum of pyridine and the thermodynamic properties of pyridine vapors. *The Journal of Chemical Physics*, 12(7), 1944.
- [37] H Knözinger and Ph Ratnasamy. Catalytic aluminas: surface models and characterization of surface sites. *Catalysis Reviews Science and Engineering*, 17(1):31–70, 1978.
- [38] M. Kobayashi and T. Shirasaki. The chemisorption of co on ruthenium metals and ruthenium-silica catalysts. *Journal of Catalysis*, 28(2):289 – 295, 1973.
- [39] C. Larese, J. M. Campos-Martin, , and J. L. G. Fierro\*. Alumina- and zirconiaalumina-loaded tinplatinum. surface features and performance for butane dehydrogenation. *Langmuir*, 16(26):10294–10300, 2000.
- [40] Xinsheng Liu. Drifts study of surface of  $\gamma$ -alumina and its dehydroxylation. *The Journal of Physical Chemistry C*, 112(13):5066–5073, 2008.

- [41] Xinsheng Liu and Ralph E Truitt. Drft-ir studies of the surface of  $\gamma$ -alumina. *Journal of the American Chemical Society*, 119(41):9856–9860, 1997.
- [42] Zhiming Liu and Seong Ihl Woo. Recent advances in catalytic denox science and technology. *Catalysis Reviews*, 48(1):43–89, 2006.
- [43] Eric Marceau, Xavier Carrier, and Michel Che. *Impregnation and Drying*, pages 59–82. Wiley-VCH Verlag GmbH Co. KGaA, 2009.
- [44] C Martin, I Martin, V Rives, G Solana, V Loddo, L Palmisano, and A Sclafani. Physicochemical characterization of wo3/zro2 and wo3/nb2o5 catalysts and their photoactivity for 4-nitrophenol photooxidation in aqueous dispersion. *Journal of materials science*, 32(22):6039–6047, 1997.
- [45] RW McCabe, C Wong, and HS Woo. The passivating oxidation of platinum. *Journal of Catalysis*, 114(2):354–367, 1988.
- [46] Isao Mochida, Seiki Kisamori, Motohiro Hironaka, Shizuo Kawano, Yuji Matsumura, and Masaaki Yoshikawa. Oxidation of no into no2 over active carbon fibers. *Energy & Fuels*, 8(6):1341–1344, 1994.
- [47] Claudio Morterra and Giuliana Magnacca. A case study: surface chemistry and surface structure of catalytic aluminas, as studied by vibrational spectroscopy of adsorbed species. *Catalysis Today*, 27(3):497–532, 1996.
- [48] Rachel L Muncrief, Karen S Kabin, and Michael P Harold. Nox storage and reduction with propylene on pt/bao/alumina. *AIChE journal*, 50(10):2526–2540, 2004.
- [49] J. W. Niemantsverdriet. *Diffraction and Extended X-Ray Absorption Fine Structure (EXAFS)*, pages 147–177. Wiley-VCH Verlag GmbH Co. KGaA, 2007.
- [50] J. W. Niemantsverdriet. *Microscopy and Imaging*, pages 179–216. Wiley-VCH Verlag GmbH Co. KGaA, 2007.
- [51] J. W. Niemantsverdriet. *Temperature-Programmed Techniques*, pages 11–38. Wiley-VCH Verlag GmbH Co. KGaA, 2007.
- [52] J. W. Niemantsverdriet. *Vibrational Spectroscopy*, pages 217–249. Wiley-VCH Verlag GmbH Co. KGaA, 2007.
- [53] MK Oudenhuijzen, JH Bitter, and DC Koningsberger. The nature of the pt-h bonding for strongly and weakly bonded hydrogen on platinum. a xafs

- spectroscopy study of the pt-h antibonding shaperesonance and pt-h exafs. *The Journal of Physical Chemistry B*, 105(20):4616–4622, 2001.
- [54] Young-Il Pae and Jong-Rack Sohn. Effect of al<sub>2</sub>o<sub>3</sub> addition and wo<sub>3</sub> modification on catalytic activity of nio/al<sub>2</sub>o<sub>3</sub>-tio<sub>2</sub>/wo<sub>3</sub> for ethylene dimerization. *Bulletin of the Korean Chemical Society*, 28(10):1763–1770, 2007.
- [55] E.P. Parry. An infrared study of pyridine adsorbed on acidic solids. characterization of surface acidity. *Journal of Catalysis*, 2(5):371 – 379, 1963.
- [56] W Przystajko, R Fiedorow, and IG Dalla Lana. Surface properties of sulphate-containing aluminas. *Applied catalysis*, 15(2):265–275, 1985.
- [57] John Regalbuto. Taylor Francis, 2007.
- [58] J.R. Regalbuto, T.H. Fleisch, and E.E. Wolf. An integrated study of pt/wo<sub>3</sub>/sio<sub>2</sub> catalysts for the no-co reaction. *Journal of Catalysis*, 107(1):114 – 128, 1987.
- [59] Hui Ren, Michael P Humbert, Carl A Menning, Jingguang G Chen, Yuying Shu, Udayshankar G Singh, and Wu-Cheng Cheng. Inhibition of coking and co poisoning of pt catalysts by the formation of au/pt bimetallic surfaces. *Applied Catalysis A: General*, 375(2):303–309, 2010.
- [60] RM Rioux and MA Vannice. Dehydrogenation of isopropyl alcohol on carbon-supported pt and cu-pt catalysts. *Journal of Catalysis*, 233(1):147–165, 2005.
- [61] Julian RH Ross. *Heterogeneous catalysis: fundamentals and applications*. Elsevier, 2011.
- [62] Joseph A Rossin. Effects of pretreatment conditions on the activity of a pt/al<sub>2</sub>o<sub>3</sub> catalyst for the oxidation of di (n-propyl) sulfide. *Journal of molecular catalysis*, 58(3):363–372, 1990.
- [63] Sounak Roy and Alfons Baiker. No x storage- reduction catalysis: From mechanism and materials properties to storage- reduction performance. *Chemical Reviews*, 109(9):4054–4091, 2009.
- [64] Sounak Roy, MS Hegde, and Giridhar Madras. Catalysis for nox abatement. *Applied Energy*, 86(11):2283–2297, 2009.
- [65] M. Steven Shackley. *An Introduction to X-Ray Fluorescence (XRF) Analysis in Archaeology*, pages 7–44. Springer New York, New York, NY, 2011.



- [66] K. S. W. Singh, J. Rouquerol, G. Bergeret, P. Gallezot, M. Vaarkamp, D. C. Koningsberger, A. K. Datye, J. W. Niemantsverdriet, T. Butz, G. Engelhardt, G. Mestl, H. Knözinger, and H. Jobic. *Characterization of Solid Catalysts: Sections 3.1.1 – 3.1.3*, pages 427–582. Wiley-VCH Verlag GmbH, 2008.
- [67] Kinga Skalska, Jacek S Miller, and Stanislaw Ledakowicz. Trends in no<sub>x</sub> abatement: a review. *Science of the Total Environment*, 408(19):3976–3989, 2010.
- [68] Lawrence Spenadel and Michel Boudart. Dispersion of platinum on supported catalysts. *The Journal of Physical Chemistry*, 64(2):204–207, 1960.
- [69] Debbie J Stokes. *Principles of SEM*, pages 17–62. John Wiley Sons, Ltd, 2008.
- [70] Kozo Tanabe. Surface and catalytic properties of zro<sub>2</sub>. *Materials Chemistry and Physics*, 13(3-4):347–364, 1985.
- [71] Michael Thiemann, Erich Scheibler, and Karl Wilhelm Wiegand. Nitric acid, nitrous acid, and nitrogen oxides. *Ullmann's encyclopedia of industrial chemistry*, 2000.
- [72] Arnaud Travert, Alexandre Vimont, Azziz Sahibed-Dine, Marco Daturi, and Jean-Claude Lavalley. Use of pyridine ch (d) vibrations for the study of lewis acidity of metal oxides. *Applied Catalysis A: General*, 307(1):98–107, 2006.
- [73] Monica Trueba and Stefano P. Trasatti.  $\gamma$ -alumina as a support for catalysts: A review of fundamental aspects. *European Journal of Inorganic Chemistry*, 2005(17):3393–3403, 2005.
- [74] Monica Trueba and Stefano P Trasatti.  $\gamma$ -alumina as a support for catalysts: A review of fundamental aspects. *European journal of inorganic chemistry*, 2005(17):3393–3403, 2005.
- [75] Alexandre Vimont, Frederic Thibault-Starzyk, and Marco Daturi. Analysing and understanding the active site by ir spectroscopy. *Chem. Soc. Rev.*, 39:4928–4950, 2010.
- [76] Alexandre Vimont, Frederic Thibault-Starzyk, and Marco Daturi. Analysing and understanding the active site by ir spectroscopy. *Chem. Soc. Rev.*, 39:4928–4950, 2010.

- [77] J Völter, G Lietz, H Spindler, and H Lieske. Role of metallic and oxidic platinum in the catalytic combustion of n-heptane. *Journal of Catalysis*, 104(2):375–380, 1987.
- [78] Paul A Webb. Introduction to chemical adsorption analytical techniques and their applications to catalysis. *Micromeritics Instrument Corp. Technical Publications*, 2003.
- [79] Brian M Weiss, Nancy Artioli, and Enrique Iglesia. Catalytic no oxidation pathways and redox cycles on dispersed oxides of rhodium and cobalt. *ChemCatChem*, 4(9):1397–1404, 2012.
- [80] X Wu, BC Gerstein, and TS King. Characterization of silica-supported ruthenium catalysts by hydrogen chemisorption and nuclear magnetic resonance of adsorbed hydrogen. *Journal of Catalysis*, 118(1):238–254, 1989.
- [81] Yoshiteru Yazawa, Noriko Kagi, Shin-ichi Komai, Atsushi Satsuma, Yuichi Murakami, and Tadashi Hattori. Kinetic study of support effect in the propane combustion over platinum catalyst. *Catalysis letters*, 72(3-4):157–160, 2001.
- [82] Yoshiteru Yazawa, Nobuyuki Takagi, Hisao Yoshida, Shin-ichi Komai, Atsushi Satsuma, Tsunehiro Tanaka, Satohiro Yoshida, and Tadashi Hattori. The support effect on propane combustion over platinum catalyst: control of the oxidation-resistance of platinum by the acid strength of support materials. *Applied Catalysis A: General*, 233(1):103–112, 2002.
- [83] R. Zhang, J. Jagiello, J.F. Hu, Z.-Q. Huang, J.A. Schwarz, and A. Datye. Effect of  $\text{wo}_3$  loading on the surface acidity of  $\text{wo}_3/\text{al}_2\text{o}_3$  composite oxides. *Applied Catalysis A: General*, 84(2):123 – 139, 1992.

# Appendix A

## Calculation for catalyst preparation

**Table A.1:** A summary of measured amounts of chemicals required for preparing catalyst with 1wt%W and 1wt%Pt

Property	Tungsten	Platinum
Chemical formula	$\text{H}_{20}\text{N}_{10}\text{W}_{12}\cdot\text{H}_2\text{O}$	$\text{Pt}(\text{NO}_3)_4$
Physical state	Solid	Solution
Molecular weight	3042.56	443.1036

### A.1 Catalyst preparation

NO oxidation catalyst with 1wt%Pt on  $\gamma$ -alumina was prepared by one step incipient wetness impregnation of  $\gamma$ -alumina with an aqueous solution of platinum nitrate,  $\text{Pt}(\text{NO}_3)_4$ . The platinum precursor contained 15% platinum. Calcination to obtain the amount of distilled water and precursor needed for one step incipient impregnation of 10g  $\gamma$ -alumina support to get 1wt% loading of Pt are shown below

$$\text{Amount of metal required} = \frac{m_{Pt}}{m_{Pt} + m_{Support}}$$

$$\frac{m_{Pt}}{m_{Pt} + m_{Support}} = 0.1$$

$$m_{Support} = \frac{0.99}{0.01} m_{Pt}$$

$$m_{Support} = 9.9g$$

$$m_{Pt} = \frac{0.01}{0.99} m_{Support}$$

$$m_{Pt} = 0.1g$$

$$\text{Pore volume of alumina support} = 1.345 \frac{cm^3}{g_{Al_2O_3}}$$

$$\text{Incipient wetness point} = 13.32 cm^3$$

$$\text{Mass required precursor} = \frac{0.1g}{0.15} m_{precursor} = 0.667g$$

$$m_{precursor\ liquid} = 0.567$$

$$\text{Amount water required} = x \cdot m_{Al_2O_3} - y \text{ cm}^3 \text{ precursor liquid}$$

$$y = \frac{m_{Pt(NO_3)_4}}{\rho_{Pt(NO_3)_4}}$$

Due to lack of density for the precursor, platinum nitrate precursor was weighted, before it was diluted with deionized water to reach required volume for impregnation. A summary of measured catalyst can be seen in Table A.2

**Table A.2:** A summary of measured amounts of chemicals required for preparing catalyst with 1wt%Pt.

Component	Amount [g]
$\gamma$ -Al <sub>2</sub> O <sub>3</sub>	9.9029
Pt-precursor	0.6750
water	13.35

## A.2 Pre-modification

Pre-modified catalyst with 1.3wt% W and 1wt%Pt on  $\gamma$ -alumina was prepared by two step incipient wetness impregnation of  $\gamma$ -alumina, first with an aqueous solution of Ammonium tungsten oxide hydrate,  $H_{20}N_{10}W_{12} \cdot xH_2O$ , then an aqueous solution of platinum nitrate,  $Pt(NO_3)_4$ . The platinum precursor contained 15% platinum. Calculations to obtain the amount of distilled water and precursor needed for impregnation of  $\gamma$ -alumina support to get 3g of 1.3wt% $WO_3$ -1wt%Pt catalyst are shown below. Prior to dissolving tungsten salt in dionized water,  $H_{20}N_{10}W_{12} \cdot xH_2O$  was dried for 2h at 100°C to remove any adsorbed water to ensure an accurate estimation of incipient wetness impregnation calculations. A summary of measurement data for tungsten impregnation can be seen in Table A.3

$$\text{Amount of metal required} = \frac{m_W}{m_{WO_3} + m_{(\text{future Pt+Support})}} \cdot m_{(\text{future Pt+Support})}$$

$$m_{WO_3} = 0.039g$$

$$n_{WO_3} = \frac{m_{WO_3}}{M_{WO_3}}$$

$$M_{WO_3} = 231.84 \frac{g}{mole}$$

$$n_{WO_3} = 0.000168 moles$$

$$n_{WO_3} = 12 \cdot n_{H_{20}N_{10}W_{12}}$$

$$m_{H_{20}N_{10}W_{12}} = \frac{1}{12} \cdot n_W \cdot M_{H_{20}N_{10}W_{12}}$$

$$m_{H_{20}N_{10}W_{12}} = 0.04265g$$

$$\text{Pore volume of alumina support} = 1.345 \frac{cm^3}{g_{Al_2O_3}}$$

$$m_{Support} = 2.931g \text{ Incipient wetness point} = 3.942cm^3$$

**Table A.3:** A summary of measured amounts of chemicals required for preparing catalyst with 1.3wt%WO<sub>3</sub> and 1wt%Pt.

Component	Amount[g]
$\gamma$ -Al <sub>2</sub> O <sub>3</sub>	2.9402
Tungsten salt	0.0416
Pt-precursor	0.6750
water	4.0451

For Platinum impregnation, same procedure as for Appendix A.1 was used, but with a pore volume of  $1.3275 \frac{cm^3}{g_{\gamma-Al_2O_3}}$ , as mentioned in Appendix B. Measurements data can be seen in Table A.4

$$m_{W/Al_2O_3} = 2.5535g$$

$$m_{Pt} = \frac{0.01}{0.99} \cdot m_{WO_3/Al_2O_3}$$

$$m_{Pt \text{ precursor}} = 0.172$$

$$\text{Incipient wetness point} = 3.3898cm^3$$

**Table A.4:** A summary of measured amounts of chemicals required for modification of WAl<sub>2</sub>O<sub>3</sub> with 1wt%Pt.

Component	Amount[g]
WAl <sub>2</sub> O <sub>3</sub>	2.5535
Pt-precursor	0.1719
water	3.39

### A.3 Post-modification

Post modified catalyst with 1wt%Pt and 1wt%W on  $\gamma$ -alumina was prepared by a one step incipient wetness impregnation of 1wt%Pt/Al<sub>2</sub>O<sub>3</sub>, prepared in

Appendix A.1. Amount of tungsten was found by the same procedure as mentioned in Appendix A.2, but with some modifications given below. A summary of measured catalyst can be seen in Table A.5

$$\begin{aligned}
 m_{\text{support}} &= m_{\text{Pt}/\text{Al}_2\text{O}_3} \\
 m_{\text{Pt}/\text{Al}_2\text{O}_3} &= 1.98g \\
 m_{\text{H}_{20}\text{N}_{10}\text{W}_{12}} &= 0.0276g \\
 \text{Incipient wetness point} &= 2.663\text{cm}^3
 \end{aligned}$$

**Table A.5:** A summary of measured amounts of chemicals required for modification of  $\text{PtAl}_2\text{O}_3$  with 1wt% $\text{WO}_3$ .

Component	Amount[g]
$\text{PtAl}_2\text{O}_3$	1.9995
Tungsten salt	0.0268
water	2.6880





## Appendix B

# Pore volume measurements

The pore volume after calcination of  $\gamma$ -alumina was found by first measuring the weight of alumina, before applying water until it was wet, but without any excess of free water. It is assumed that 1g of water corresponds to 1cm<sup>3</sup>, and pore volume was found by dividing volume of water used by weight of alumina. This was done in 3 parallels, and all data can be seen in Table B.1.

**Table B.1:** Data used for finding pore volume of alumina.

Parallel	Pore volume [ $\frac{cm^3}{g}$ ]
Parallel 1	1.354
Parallel 2	1.339
Parallel 3	1.342
Average	1.345

For pre-modified catalyst, W/Al<sub>2</sub>O<sub>3</sub> was transferred into a small mortar and weighted, before deionized water was introduced. This was done until complete wetting was achieved, and the sample was weighted again. The difference in weight stem from water, and measured data can be seen in Table B.2. After pore volume measurements, W/Al<sub>2</sub>O<sub>3</sub> was dried at 100°C to remove water. Due to this, only one sample was measured.

**Table B.2:** Data used for finding pore volume of W/Al<sub>2</sub>O<sub>3</sub>.

Parallel	Pore volume [ $\frac{cm^3}{g}$ ]
Parallel 3	1.3275
Average	1.3275

## Appendix C

# Nitrogen adsorption

A representation of the Nitrogen adsorption isotherm and pore size distribution is given below.

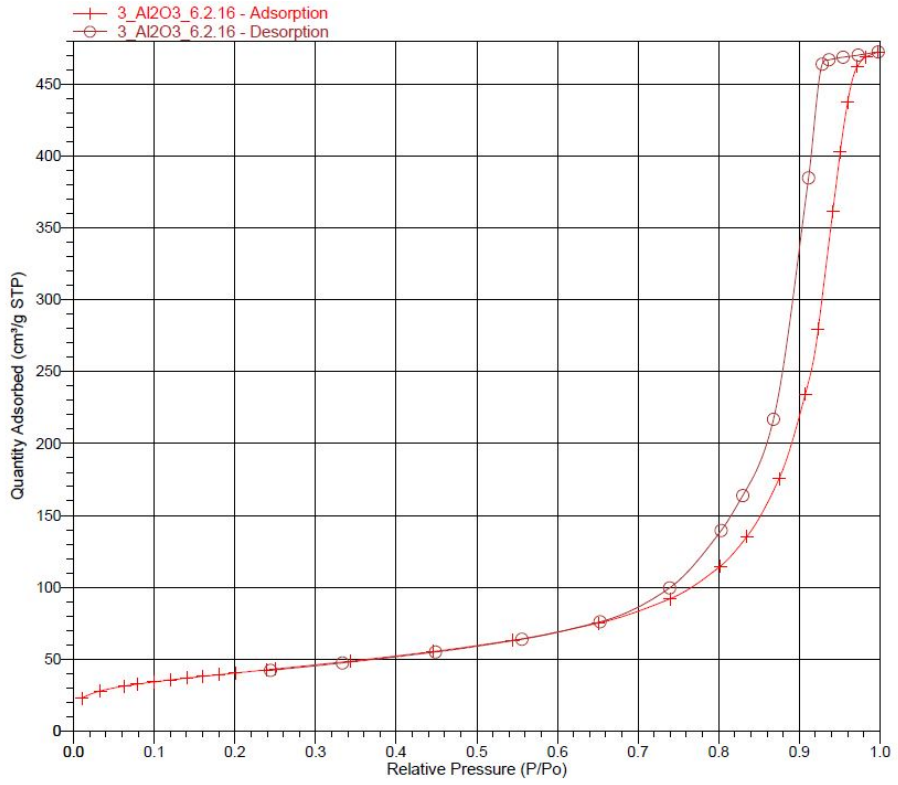


Figure C.1: The The adsorption/desorption curve for  $\gamma$ - $\text{Al}_2\text{O}_3$

APPENDIX C. NITROGEN ADSORPTION

---

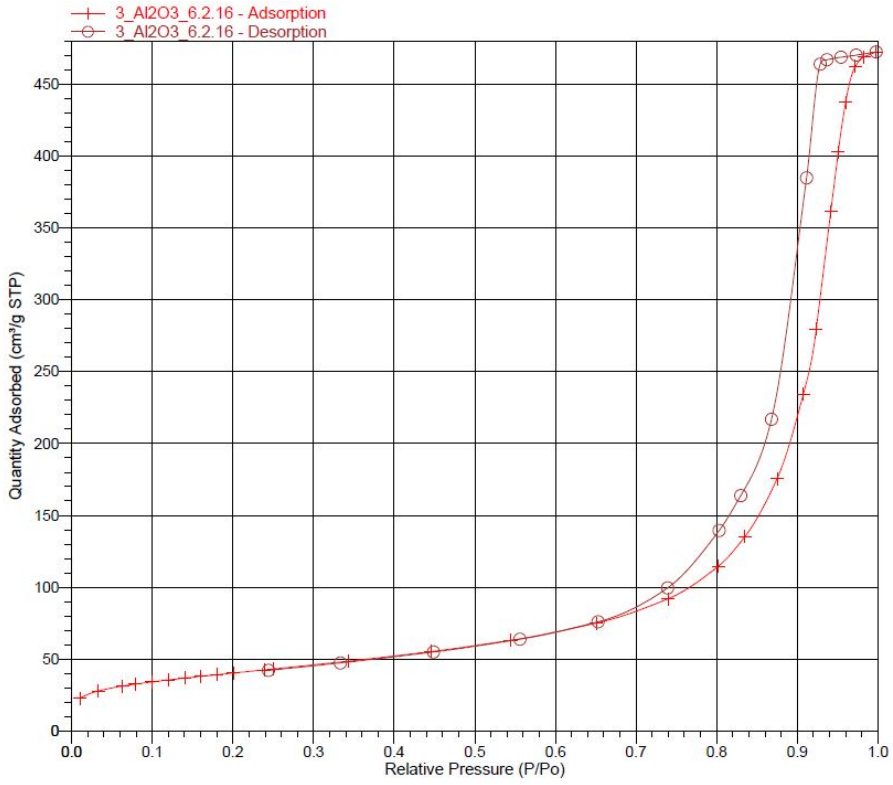


Figure C.2: Pore size distribution for  $\gamma$ -Al<sub>2</sub>O<sub>3</sub>

*APPENDIX C. NITROGEN ADSORPTION*

---

## Appendix D

# Chemisorption Sequence and Isotherms

### D.1 Chemisorption Sequence

Chemisorption measurements for the different catalyst, as well as a representation of the isotherms.

**Table D.1:** H<sub>2</sub> Chemisorption Analysis conditions and sequences for Pt/Al<sub>2</sub>O<sub>3</sub>.

Task number	Analysis step	Temp[°C]	Time[min]
1	Evacuation	110	30
2	Leak Test	100	
3	Hydrogen Flow	100	10
4	Hydrogen Flow	600	120
5	Evacuation	600	120
6	Evacuation	35	30
7	Leak test	35	
8	Evacuation	35	20
9	Analysis	35	

D.2.

**Table D.2:** CO Chemisorption Analysis conditions and sequences for Pt/Al<sub>2</sub>O<sub>3</sub>.

Task number	Analysis step	Temp[°C]	Time[min]
1	Evacuation	40	60
2	Leak Test	40	
3	Hydrogen Flow	600	120
4	Evacuation	580	60
5	Evacuation	100	45
6	Leak test	100	
7	Evacuation	50	60
8	Analysis	35	

**Table D.3:** H<sub>2</sub> Chemisorption Analysis conditions and sequences for Ru/Al<sub>2</sub>O<sub>3</sub>.

Task number	Analysis step	Temp[°C]	Time[min]
1	Evacuation	35	120
2	Evacuation	400	20
3	Leak test	400	
4	Hydrogen Flow	400	120
5	Evacuation	400	120
6	Evacuation	100	30
7	Leak test	100	
8	Evacuation	100	30
9	Analysis	100	

## D.2

### Chemisorption Isotherm



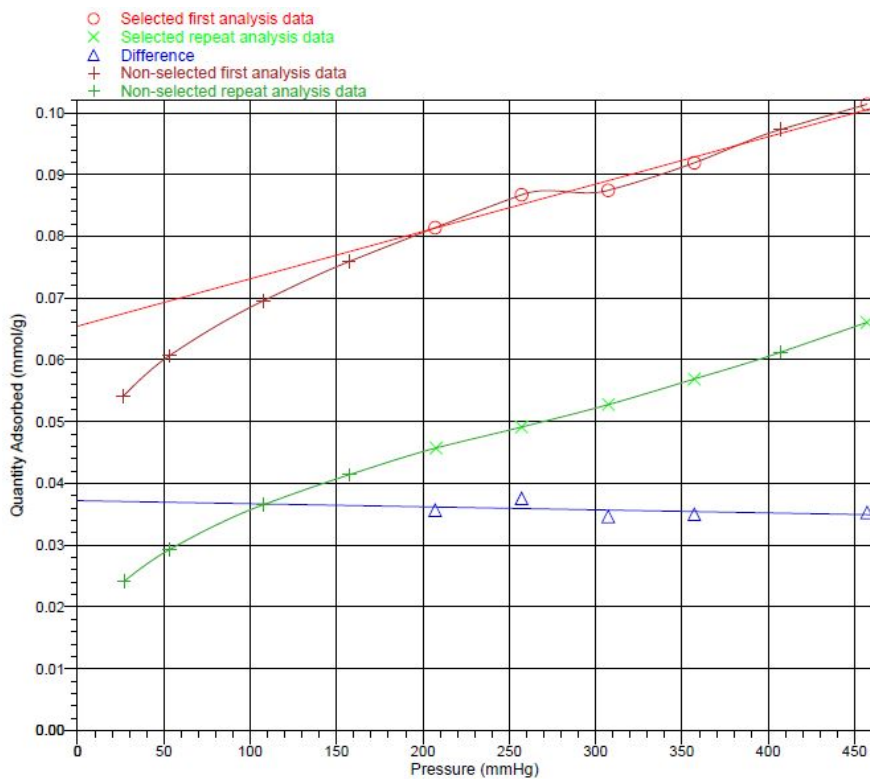


**Figure D.1:** Pt/Al<sub>2</sub>O<sub>3</sub> The isotherm for the total adsorption with trend line in red and the isotherm in green. The blue line represents strongly adsorbed CO.

*D.2.*

*CHEMISORPTION ISOTHERM*

*APPENDIX D. CHEMISORPTION*

---

# Appendix E

## X-ray Diffraction

Profiles matching characteristic spinal reflections for individual samples can be seen in Figure E.1, E.2, E.3 and E.4. The height of spinal reflections do not necessarily reflect the measured intensity

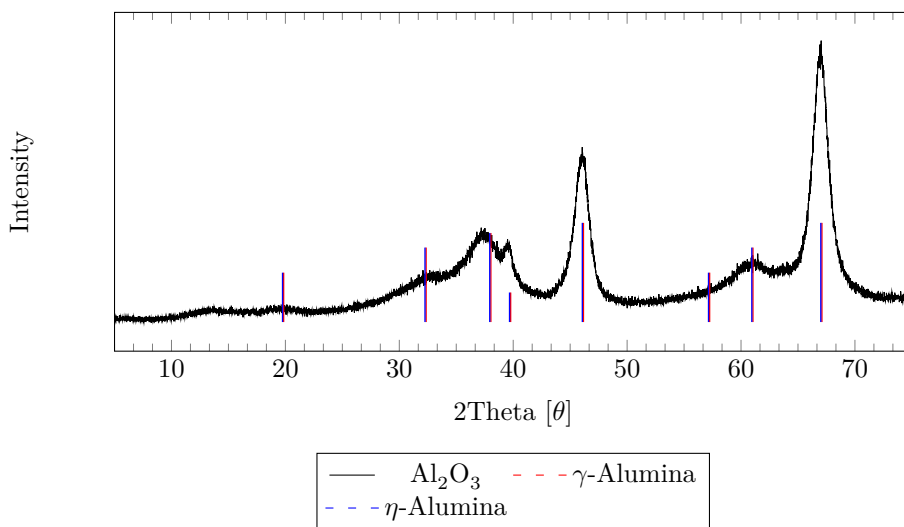


**Figure E.1:** XRD profile of  $\text{Al}_2\text{O}_3$ .

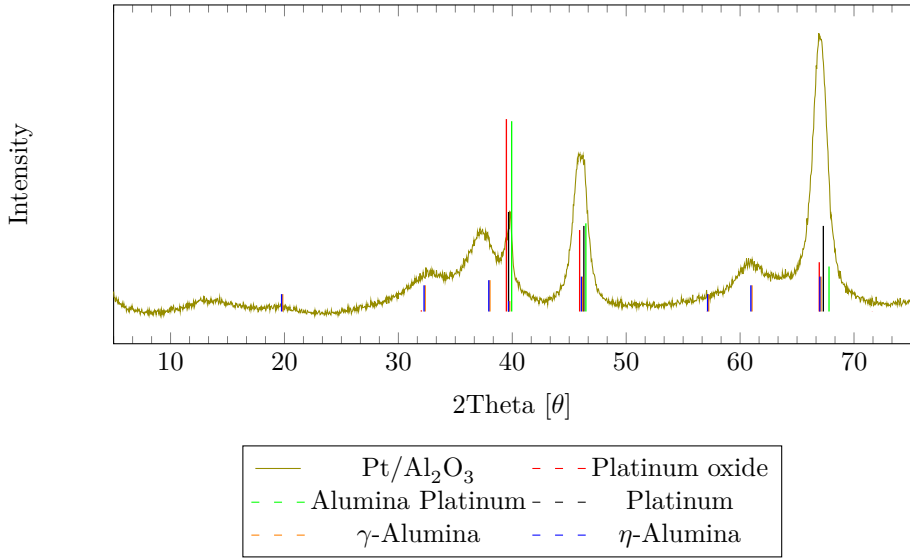


**Figure E.2:** XRD profile of Pt/Al<sub>2</sub>O<sub>3</sub>.

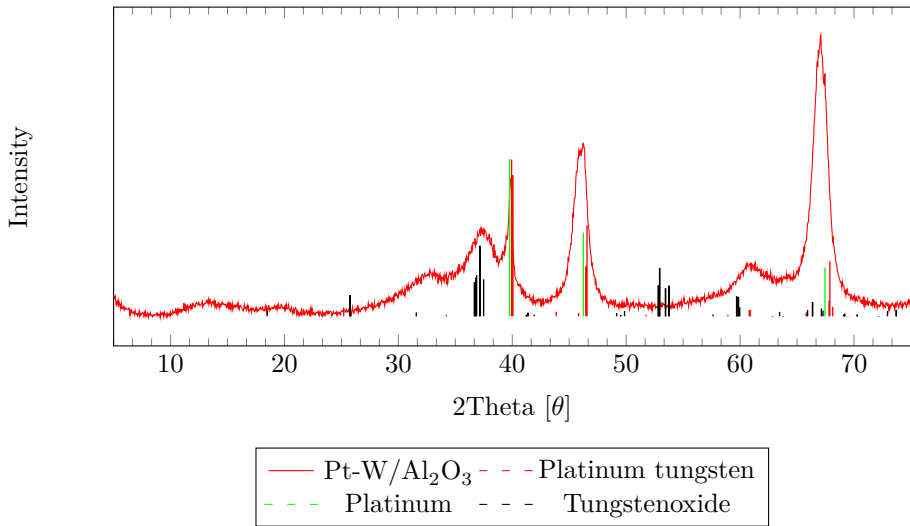


**Figure E.3:** XRD profile of Pt-W/Al<sub>2</sub>O<sub>3</sub>.

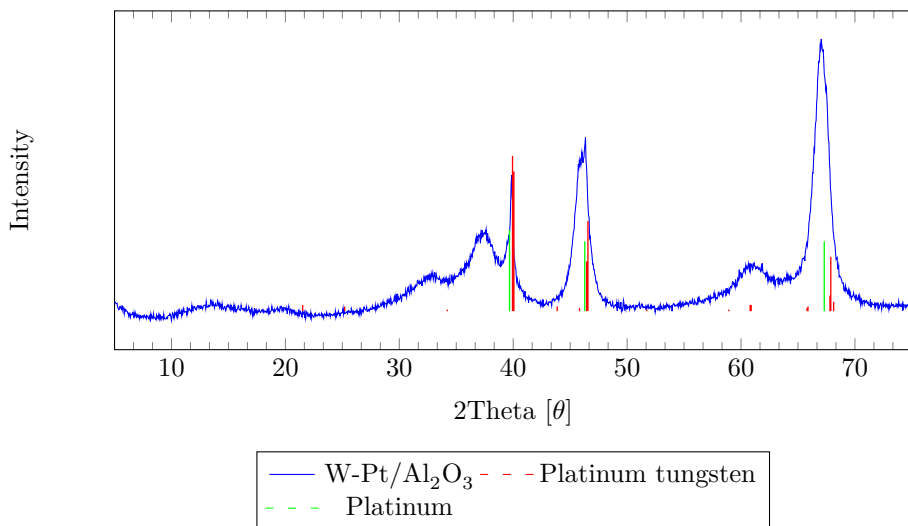


**Figure E.4:** XRD profile of W-Pt/Al<sub>2</sub>O<sub>3</sub>.



# Appendix F

## FTIR wavelength

Position of pyridine bands between  $1700\text{-}1400\text{cm}^{-1}$  upon adsorption on  $\gamma$ -alumina are given in Table F.1.

**Table F.1:** Position of pyridine bands upon adsorption on  $\gamma$ -alumina

Adsorption mode	Acids	Peaks	Strong/weak	Source
Coordinated	Lewis	1447-1460	Very strong	[55]
	Lewis	1443	weak	[41]
	Lewis	1449	medium	[41]
	lewis	1453	strong	[41]
	Lewis	1485-1500	variable	[55]
	Lewis	1580	variable	[55]
	lewis	1592	weak	[40]
	Lewis	1593	weak	[47]
	Lewis	1610-1635	unknown	[55]
	Lewis	1612	unknown	[40]
	Lewis	1614	medium	[47]
	Lewis	1621	strong	[40]
Ion	Brønstedt	1485-1500	very strong	[55]
	Brønstedt	1540-1543	strong	[55]
	Brønstedt	1620	strong	[55]
	Brønstedt	1640	strong	[55]
Hydrogen bonded		1440-1447	very strong	[55]
		1485-1490	weak	[55]
		1580-1600	strong	[55]



# Appendix G

## Risk assesment



<b>ID</b>	2781	<b>Status</b>	<b>Dato</b>
<b>Risikoområde</b>	Risikovurdering: Helse, miljø og sikkerhet (HMS)	Opprettet	18.12.2015
<b>Opprettet av</b>	Mads Alexander Lid	Vurdering startet	12.01.2016
<b>Ansvarlig</b>	Mads Alexander Lid	Tiltak besluttet	
		Avsluttet	

**CAT, Master student, 2016, Mads Alexander Lid****Gyldig i perioden:**

1/15/2016 - 6/10/2016

**Sted:**

3 - Gløshaugen / 315 - Kjemi 5

**Mål / hensikt**

This risk assessment contains all the activities that the master student Mads Alexander Lid will perform in the labs of the Catalysis group.

**Bakgrunn**

The project aims to find new catalysts for low temperature selective catalytic oxidation (SCO) of NOx. Pt/Al<sub>2</sub>O<sub>3</sub> seems to be a good candidate, and the catalyst has to be prepared for characterization and analysis.

**Beskrivelse og avgrensninger**

The catalyst will be prepared by impregnating Alumina (Al<sub>2</sub>O<sub>3</sub>) with platinum nitrate, and drying off the solvent. Catalyst will then be impregnated with Ammonium tungsten oxide hydrate, and drying off the solvent.

**Forutsetninger, antakelser og forenklinger**

[Ingen registreringer]

**Vedlegg**

[Ingen registreringer]

**Referanser**

[Ingen registreringer]

**Oppsummering, resultat og endelig vurdering**

I oppsummeringen presenteres en oversikt over farer og uønskede hendelser, samt resultat for det enkelte konsekvensområdet.

**Farekilde: Use of furnaces****Uønsket hendelse: Burn from hot furnace**

<b>Konsekvensområde:</b> Helse	Risiko før tiltak:	Risiko etter tiltak:
Ytre miljø	Risiko før tiltak:	Risiko etter tiltak:
Materielle verdier	Risiko før tiltak:	Risiko etter tiltak:

**Farekilde: Preparation of precursor solution and impregnation of alumina support****Uønsket hendelse: Chemical burn**

<b>Konsekvensområde:</b> Helse	Risiko før tiltak:	Risiko etter tiltak:
Ytre miljø	Risiko før tiltak:	Risiko etter tiltak:
Materielle verdier	Risiko før tiltak:	Risiko etter tiltak:

**Uønsket hendelse: Formation of harmful chemicals/gas**

<b>Konsekvensområde:</b> Helse	Risiko før tiltak:	Risiko etter tiltak:
Ytre miljø	Risiko før tiltak:	Risiko etter tiltak:
Materielle verdier	Risiko før tiltak:	Risiko etter tiltak:

**Uønsket hendelse: Spill of platina precursor onto skin**

<b>Konsekvensområde:</b> Helse	Risiko før tiltak:	Risiko etter tiltak:
Ytre miljø	Risiko før tiltak:	Risiko etter tiltak:
Materielle verdier	Risiko før tiltak:	Risiko etter tiltak:

**Uønsket hendelse: inhalation of powders**

<b>Konsekvensområde:</b> Helse	Risiko før tiltak:	Risiko etter tiltak:
--------------------------------	--------------------	----------------------

**Uønsket hendelse: Use of oil bath**

<b>Konsekvensområde:</b> Helse	Risiko før tiltak:	Risiko etter tiltak:
--------------------------------	--------------------	----------------------



**Farekilde:** In-situ DRIFTS using Pyridine Adsorption

**Uønsket hendelse:** Leakage

**Konsekvensområde:** Helse

Risiko før tiltak: Risiko etter tiltak:

**Uønsket hendelse:** Fire during heating treatment

**Konsekvensområde:** Helse  
Ytre miljø  
Materielle verdier

Risiko før tiltak: Risiko etter tiltak:   
Risiko før tiltak: Risiko etter tiltak:   
Risiko før tiltak: Risiko etter tiltak:

**Uønsket hendelse:** Electric shock

**Konsekvensområde:** Helse

Risiko før tiltak: Risiko etter tiltak:

**Uønsket hendelse:** Uncontrolled heating

**Konsekvensområde:** Helse  
Ytre miljø  
Materielle verdier

Risiko før tiltak: Risiko etter tiltak:   
Risiko før tiltak: Risiko etter tiltak:   
Risiko før tiltak: Risiko etter tiltak:

**Endelig vurdering**



**Oversikt involverte enheter og personell**

En risikovurdering kan gjelde for en, eller flere enheter i organisasjonen. Denne oversikten presenterer involverte enheter og personell for gjeldende risikovurdering.

**Enhet /-er risikovurderingen omfatter**

- Institutt for kjemisk prosesseteknologi

**Deltakere**

Magnus Rønning  
Cristian Ledesma Rodriguez  
Karin Wiggen Dragsten

**Lesere**

[Ingen registreringer]

**Andre involverte/interessenter**

[Ingen registreringer]

**Følgende akseptkriterier er besluttet for risikoområdet Risikovurdering: Helse, miljø og sikkerhet (HMS):**

**Helse**



**Materielle verdier**



**Omdømme**



**Ytre miljø**



**Oversikt over eksisterende, relevante tiltak som er hensyntatt i risikovurderingen**

I tabellen under presenteres eksisterende tiltak som er hensyntatt ved vurdering av sannsynlighet og konsekvens for aktuelle uønskede hendelser.

Farekilde	Ønsket hendelse	Tiltak hensyntatt ved vurdering
Use of furnaces	Burn from hot furnace	Heat-resistant gloves
Preparation of precursor solution and impregnation of alumina support	Chemical burn	Safety Goggles
	Chemical burn	Lab Coat
	Chemical burn	Fume hoods
	Chemical burn	Nitrile gloves
	Formation of harmful chemicals/gas	Safety Goggles
	Formation of harmful chemicals/gas	Lab Coat
	Formation of harmful chemicals/gas	Fume hoods
	Formation of harmful chemicals/gas	Nitrile gloves
	Spill of platina precursor onto skin	Safety Goggles
	Spill of platina precursor onto skin	Lab Coat
	Spill of platina precursor onto skin	Fume hoods
	Spill of platina precursor onto skin	Nitrile gloves
	Spill of platina precursor onto skin	Emergency Eye shower and flask
	Spill of platina precursor onto skin	Emergency shower
	inhalation of powders	Fume hoods
Use of oil bath	Heat-resistant gloves	
In-situ DRIFTS using Pyridine Adsorption	Leakage	Safety Goggles
	Leakage	Lab Coat
	Leakage	Fume hoods
	Leakage	Emergency Eye shower and flask
	Leakage	Emergency shower
	Leakage	Fire Extinguisher
	Leakage	Tightening connections/cover with parafilm
	Fire during heating treatment	Emergency shower
	Fire during heating treatment	Fire Extinguisher
	Electric shock	
Uncontrolled heating		



**Eksisterende og relevante tiltak med beskrivelse:**

**Heat-resistant gloves**

Using furnaces to calcine the support and impregnated catalyst. Protection against burns

**Safety Goggles**

Eye protection to be worn at all times while working in lab.

**Lab Coat**

Protection of skin against spills, corrosive chemicals, etc.

**Fume hoods**

Platinum nitrate can form harmful gases. Handle in fume hood

**Nitrile gloves**

Platinum nitrate is corrosive and oxidizing. Hand protection important

**Emergency Eye shower and flask**

In case chemicals come in contact with eyes. Rinse with plenty of water, consult medical personnell

**Emergency shower**

In case of serious spills, or clothing on fire. Located in lab.

**Fire Extinguisher**

[Ingen registreringer]

**Tightening connections/cover with parafilm**

[Ingen registreringer]

**Extensive flushing with N2**

Removal and dilution

**Risikoanalyse med vurdering av sannsynlighet og konsekvens**

I denne delen av rapporten presenteres detaljer dokumentasjon av de farer, uønskede hendelser og årsaker som er vurdert. Innledningsvis oppsummeres farer med tilhørende uønskede hendelser som er tatt med i vurderingen.

**Følgende farer og uønskede hendelser er vurdert i denne risikovurderingen:**

- **Use of furnaces**
  - Burn from hot furnace
- **Preparation of precursor solution and impregnation of alumina support**
  - Chemical burn
  - Formation of harmful chemicals/gas
  - Spill of platina precursor onto skin
  - inhalation of powders
  - Use of oil bath
- **In-situ DRIFTS using Pyridine Adsorption**
  - Leakage
  - Fire during heating treatment
  - Electric shock
  - Uncontrolled heating

**Oversikt over besluttede risikoreduserende tiltak med beskrivelse:****Use of furnaces (farekilde)**

Alumina will be calcined in HT-furnaces  
Catalyst/impregnated alumina will be dried/calcined in furnaces

**Use of furnaces/Burn from hot furnace (uønsket hendelse)**

Accidentally touching a hot surface on the furnace may cause burns.

Samlet sannsynlighet vurdert for hendelsen: Lite sannsynlig (2)

Kommentar til vurdering av sannsynlighet:

[Ingen registreringer]

**Vurdering av risiko for følgende konsekvensområde: Helse**

Vurdert sannsynlighet (felles for hendelsen): Lite sannsynlig (2)

Vurdert konsekvens: Middels (2)

Kommentar til vurdering av konsekvens:

[Ingen registreringer]





**Preparation of precursor solution and impregnation of alumina support (farekilde)**

Diluting Platinum nitrate solution, and impregnating alumina

**Preparation of precursor solution and impregnation of alumina support/Chemical burn (uønsket hendelse)**

Platinum nitrate is corrosive and oxidising.

Samlet sannsynlighet vurdert for hendelsen: Lite sannsynlig (2)

Kommentar til vurdering av sannsynlighet:

[Ingen registreringer]

**Vurdering av risiko for følgende konsekvensområde: Helse**

Vurdert sannsynlighet (felles for hendelsen): Lite sannsynlig (2)

Vurdert konsekvens: Middels (2)

Kommentar til vurdering av konsekvens:

[Ingen registreringer]

**Preparation of precursor solution and impregnation of alumina support/Formation of harmful chemicals/gas (uønsket hendelse)**

Platinum nitrate may react and form harmful gas.

Samlet sannsynlighet vurdert for hendelsen: Sannsynlig (3)

Kommentar til vurdering av sannsynlighet:

[Ingen registreringer]

**Vurdering av risiko for følgende konsekvensområde: Helse**

Vurdert sannsynlighet (felles for hendelsen): Sannsynlig (3)

Vurdert konsekvens: Middels (2)

Kommentar til vurdering av konsekvens:

[Ingen registreringer]





**Preparation of precursor solution and impregnation of alumina support/Spill of platina precursor onto skin (uønsket hendelse)**

Samlet sannsynlighet vurdert for hendelsen: Sannsynlig (3)

Kommentar til vurdering av sannsynlighet:

[Ingen registreringer]

**Vurdering av risiko for følgende konsekvensområde: Helse**

Vurdert sannsynlighet (felles for hendelsen): Sannsynlig (3)

Vurdert konsekvens: Stor (3)

Kommentar til vurdering av konsekvens:

[Ingen registreringer]



**Preparation of precursor solution and impregnation of alumina support/inhalation of powders (uønsket hendelse)**

Samlet sannsynlighet vurdert for hendelsen: Lite sannsynlig (2)

Kommentar til vurdering av sannsynlighet:

[Ingen registreringer]

**Vurdering av risiko for følgende konsekvensområde: Helse**

Vurdert sannsynlighet (felles for hendelsen): Lite sannsynlig (2)

Vurdert konsekvens: Middels (2)

Kommentar til vurdering av konsekvens:

[Ingen registreringer]





**Preparation of precursor solution and impregnation of alumina support/Use of oil bath (uønsket hendelse)**

Årsak: Burns

Beskrivelse:

Samlet sannsynlighet vurdert for hendelsen: Lite sannsynlig (2)

Kommentar til vurdering av sannsynlighet:

[Ingen registreringer]

**Vurdering av risiko for følgende konsekvensområde: Helse**

Vurdert sannsynlighet (felles for hendelsen): Lite sannsynlig (2)

Vurdert konsekvens: Middels (2)

Kommentar til vurdering av konsekvens:

[Ingen registreringer]



**In-situ DRIFTS using Pyridine Adsorption (farekilde)**

Infrared spectra were collected using the OMNIC v.9.0 software in connection with a 912A0763 Nicolet iS50 FTIR KBr Gold Spectrometer and pyridine

**In-situ DRIFTS using Pyridine Adsorption/Leakage (uøsket hendelse)**

Leakage of pyridine into the surrounding area.

*Årsak:* Bad Connection between bubbler and pipes

*Beskrivelse:*

*Årsak:* Residuals of pyridine in reaction chamber

*Beskrivelse:*

Samlet sannsynlighet vurdert for hendelsen: Sannsynlig (3)

Kommentar til vurdering av sannsynlighet:

[Ingen registreringer]

**Vurdering av risiko for følgende konsekvensområde: Helse**

Vurdert sannsynlighet (felles for hendelsen): Sannsynlig (3)

Vurdert konsekvens: Stor (3)

Kommentar til vurdering av konsekvens:

R-11 Highly flammable.  
R-20/21/22 Harmful by inhalation, in contact with skin and if swallowed.

**In-situ DRIFTS using Pyridine Adsorption/Fire during heating treatment (uøsket hendelse)**

Samlet sannsynlighet vurdert for hendelsen: Svært lite sannsynlig (1)

Kommentar til vurdering av sannsynlighet:

[Ingen registreringer]

**Vurdering av risiko for følgende konsekvensområde: Helse**

Vurdert sannsynlighet (felles for hendelsen): Svært lite sannsynlig (1)

Vurdert konsekvens: Middels (2)

Kommentar til vurdering av konsekvens:

[Ingen registreringer]





**In-situ DRIFTS using Pyridine Adsorption/Electric shock (uønsket hendelse)**

Samlet sannsynlighet vurdert for hendelsen: Svært lite sannsynlig (1)

Kommentar til vurdering av sannsynlighet:

[Ingen registreringer]

**Vurdering av risiko for følgende konsekvensområde: Helse**

Vurdert sannsynlighet (felles for hendelsen): Svært lite sannsynlig (1)

Vurdert konsekvens: Middels (2)

Kommentar til vurdering av konsekvens:

[Ingen registreringer]



**In-situ DRIFTS using Pyridine Adsorption/Uncontrolled heating (uønsket hendelse)**

Uncontrolled heating of either MS or the temperature controller.

Samlet sannsynlighet vurdert for hendelsen: Lite sannsynlig (2)

Kommentar til vurdering av sannsynlighet:

[Ingen registreringer]

**Vurdering av risiko for følgende konsekvensområde: Helse**

Vurdert sannsynlighet (felles for hendelsen): Lite sannsynlig (2)

Vurdert konsekvens: Liten (1)

Kommentar til vurdering av konsekvens:

[Ingen registreringer]





**Oversikt over besluttede risikoreducerende tiltak:**

Under presenteres en oversikt over risikoreducerende tiltak som skal bidra til å reduseres sannsynlighet og/eller konsekvens for uønskede hendelser.

**Oversikt over besluttede risikoreducerende tiltak med beskrivelse:**

